UCRL-11565

University of California

Ernest O. Lawrence Radiation Laboratory

POLARIZATION PARAMETER IN PROTON-PROTON SCATTERING FROM 328 TO 736 MeV

Berkeley, California

DISCLAIMER

Research and Development

UCRL-11565

UNIVERSITY OF CALIFORNIA

Lawrence Radiation Laboratory
Berkeley, California

AEC Contract No. W-7405-eng-48

POLARIZATION PARAMETER IN PROTON-PROTON SCATTERING FROM 328 TO 736 MeV

Frederick William Betz

(Ph. D. Thesis)

August 11, 1964

POLARIZATION PARAMETER IN PROTON-PROTON SCATTERING FROM 328 TO 736 MeV

Contents

POLARIZATION PARAMETER IN PROTON-PROTON SCATTERING FROM 328 TO 736 MeV

Frederick William Betz

Lawrence Radiation Laboratory
University of California
Berkeley, California

August 11, 1964

ABSTRACT

The polarization parameter in elastic proton-proton scattering has been measured at several energies and angles. The unpolarized external proton beam from the 184-inch synchrocyclotron was made incident upon a polarized target. The full energy of the beam was degraded by means of copper absorber to obtain beams with laboratory kinetic energies of 328, 614, 679, and 736 MeV. The elastic proton-proton scatterings were kinematically separated from background events by detection of both protons in coincidence with the use of scintillation counters. Measurements were made in the center-of-mass angular region from 33 to 110 degrees (at smaller angles the slower proton lacked sufficient range to emerge from the target). The target was polarized by means of a technique called dynamic nuclear orientation. Its polarization was measured by monitoring the nuclear magnetic resonance signal of the free protons in the target. This signal was calibrated in terms of absolute magnitude of polarization by measurement of the temperature of the proton system and the frequency of its resonance when the polarization of the target was unenhanced. The experimental procedure was to count the number of elastic scatterings into a solid angle with the polarization of the target parallel to the normal to the scattering plane and then, under identical conditions, to count the elastic scatterings with the direction of the polarization of the target reversed. The measured values of the polarization parameter are presented as a function of angle for each incident proton energy.

I. INTRODUCTION

The two-nucleon interaction is of interest in the investigation of the nature of the strong interactions and, insofar as the nuclear forces can be considered two-body interactions, in the investigation of the binding of the atomic nucleus. Since a nucleon has an intrinsic spin of 1/2, it is necessary to obtain information on the spin dependence of the interaction. This dissertation describes an experiment to obtain data on the two-nucleon (isotopic spin = 1) scattering amplitude. An unpolarized proton beam was made incident upon a polarized proton target to measure the polarization parameter $P(\theta)$ in elastic p-p scattering for lab energies from 328 to 736 MeV. Comprehensive reviews of previous work on high-energy nucleon-nucleon interaction can be found in the articles by MacGregor et al.,[1] Hess,[2] and Wolfenstein:[3] these also contain extensive lists of references.

II. THEORY

The density matrix formalism, introduced by Wolfenstein and Ashkin[4] and by Dalitz,[5] is useful for the description of scattering experiments that involve polarization.

Let ψ_i be a wave function describing the incident wave of a beam of particles upon a target. This incident wave gives rise to a scattered wave that displays a scattered amplitude in each spin state. Let ψ_f be the scattered wave, M the interaction matrix (with the part giving rise to the unscattered wave subtracted out, M = S-1, where S is the usual S matrix), and I the differential cross section of the scattering. From the definition of M

$$\psi_f = M \psi_i$$

where ψ_i is normalized, $\psi_i^\dagger \psi_i = 1$ (matrix multiplication is implied). The scattered wave ψ_f is not normalized, but

$$I = \psi_f^\dagger \psi_f$$

$$I = (M \psi_i)^\dagger M \psi_i = \psi_i^\dagger M^\dagger M \psi_i .$$

For proton-proton scattering M is a 4 ×4 matrix, ψ is a four-component column symbol, $\psi^\dagger$ is a four-component row symbol, and $\dagger$ indicates the Hermitian conjugate.

If ψ_i can be written, the initial state is completely known and may, in a sense, be said to be completely polarized. In practice, states of partial polarization must be dealt with, as when a polarized target is only 50% polarized (not 100%). States of partial polarization can be described as incoherent mixtures of states of complete polarization. As a simple example, the scattering of spin-0 particles on a spin-1/2 polarized target will be described. Suppose the target protons were in a state of partial polarization so that f_1 of the protons could be described by an initial wave function ψ_{i1} and the remainder, fraction $f_2 = 1 - f_1$, by the wave function ψ_{i2}. Then the scattered intensity would be

$$I = f_1 (M \psi_{i1})^\dagger M \psi_{i1} + f_2 (M \psi_{i2})^\dagger M \psi_{i2}$$

$$I = f_1 \psi_{i1}^\dagger M^\dagger M \psi_{i1} + f_2 \psi_{i2}^\dagger M^\dagger M \psi_{i2} \quad .$$

Similarly, if one wished to find the average value of the x component of spin σ_x for the scattered particles (final state), one calculates

$$\langle \sigma_x \rangle_f = \frac{f_1 \psi_{f1}^\dagger \sigma_x \psi_{f1} + f_2 \psi_{f2}^\dagger \sigma_x \psi_{f2}}{f_1 \psi_{f1}^\dagger \psi_{f1} + f_2 \psi_{f2}^\dagger \psi_{f2}}$$

$$\langle \sigma_x \rangle_f = \frac{f_1 \psi_{i1}^\dagger M^\dagger \sigma_x M \psi_{i1} + f_2 \psi_{i2}^\dagger M^\dagger \sigma_x M \psi_{i2}}{f_1 \psi_{i1}^\dagger M^\dagger M \psi_{i1} + f_2 \psi_{i2}^\dagger M^\dagger M \psi_{i2}} \quad ,$$

where the denominator amounts to a normalization factor.

In general, it may require more than two contributions to describe the desired state of partial polarization. If n components were required, one could use fractions $f_1 \cdots f_n$ to make up the initial state. Any state of partial polarization (or no polarization) can be made up as an incoherent mixture of perfectly polarized ingredients. For purposes of notation, this formalism can be simplified by making up a new matrix

$$\rho_i = \sum_\alpha f_\alpha \psi_{i\alpha} \psi_{i\alpha}^\dagger \quad .$$

In the simple case of two contributions,

$$\rho_i = f_1 \psi_{i1} \psi_{i1}^\dagger + f_2 \psi_{i2} \psi_{i2}^\dagger \quad .$$

If ψ_{i1} and ψ_{i2} are two-element column symbols, then ρ would be a 2×2 matrix.

If ψ_{i1} is written $\begin{pmatrix} \psi_{i11} \\ \psi_{i12} \end{pmatrix}$, where ψ_{i11} and ψ_{i12} are complex numbers, then $\psi_{i1}^\dagger$ is $(\psi_{i11}^* \ \psi_{i12}^*)$ and

$$\rho_i = f_1 \begin{pmatrix} \psi_{i11}\psi_{i11}^* & \psi_{i11}\psi_{i12}^* \\ \psi_{i12}\psi_{i11}^* & \psi_{i12}\psi_{i12}^* \end{pmatrix} + f_2 \begin{pmatrix} \psi_{i21}\psi_{i21}^* & \psi_{i21}\psi_{i22}^* \\ \psi_{i22}\psi_{i21}^* & \psi_{i22}\psi_{i22}^* \end{pmatrix} .$$

The advantage of introducing this matrix is that the forms we have used can be written very simply as

$$Tr(\rho_i) \equiv \text{Trace}\,\rho_i = 1$$
$$I = Tr(M\rho_i M^\dagger)/Tr(\rho_i) = Tr(M\rho_i M^\dagger)$$
$$I\langle\sigma_x\rangle_f = Tr(\sigma_x M \rho_i M^\dagger)$$

(Note: in deriving these relations, one uses the fact that in taking the trace of a product of matrices the product may be cyclically permuted—

$$Tr(ABC) = Tr(CAB) = Tr(BCA) \quad).$$

It is convenient to use a similar matrix to describe separately the final state

$$\rho_f = M\rho_i M^\dagger$$

$$I = Tr(\rho_f) / Tr(\rho_i)$$

$$I\langle\sigma_x\rangle_f = Tr(\sigma_x \rho_f) \quad .$$

ρ is called the density matrix. This matrix has the advantage that it is guaranteed to include all cases of partial polarization.

Since the density matrix in our simple example is a 2×2 matrix, it can be represented as a sum

$$\rho = a_0 1 + a_1\sigma_1 + a_2\sigma_2 + a_3\sigma_3 \quad ,$$

where 1 is the unit 2×2 matrix and σ_1, σ_2, σ_3 are the three Pauli spin matrices. This set is complete, since none are linear combinations of the others. It has the convenient property

$$Tr(S^\mu S^\nu) = 2\delta_{\mu\nu}$$

where S indicates one of the set: $1., \sigma_1, \sigma_2, \sigma_3$.

This formalism has the important advantage of displaying explicitly what information is needed to describe fully a state of partial polarization. If the initial density matrix describes a set of protons that are partially polarized, then ρ_i is completely determined if we know all of the a_μ in the expansion

$$\rho_i = \sum a_\mu S^\mu \quad .$$

Since $Tr(\rho_i S^\mu) = 2a_\mu$, we need to know

$$2a_0 = Tr(\rho_i) \qquad (= 1 \text{ in our case})$$
$$2a_1 = Tr(\rho_i \sigma_1) \qquad (= \langle \sigma_1 \rangle_i)$$
$$2a_2 = Tr(\rho_i \sigma_2) \qquad (= \langle \sigma_2 \rangle_i)$$
$$2a_3 = Tr(\rho_i \sigma_3) \qquad (= \langle \sigma_3 \rangle_i) \quad .$$

In the final state the similar expressions are

$$\rho_f = M \rho_i M^\dagger$$
$$I = Tr(\rho_f) / Tr(\rho_i)$$
$$I \langle \sigma_x \rangle_f = Tr(\rho_f \sigma_x) \quad .$$

In general,

$$I \langle S^\mu \rangle_f = Tr(\rho_f S^\mu) \quad .$$

In fact the whole formalism may be expressed very compactly and conveniently as

$$\rho = \tfrac{1}{2} \sum_\mu Tr(\rho S^\mu) S^\mu$$

$$\rho = \tfrac{1}{2} Tr(\rho) \sum_\mu \langle S^\mu \rangle S^\mu \quad .$$

Here $Tr(\rho)$ is a normalization factor that is equal to 1 for our ρ_i and is equal to I for our ρ_f. Furthermore $\langle S^\mu \rangle$ is the expectation value of the particular operator for the particles in the state in question. If the initial state is partially polarized, ρ_i is then determined, and we wish to express information about the final state:

$$I \langle S^\mu \rangle_f = \tfrac{1}{2} \sum_\nu \langle S^\nu \rangle_i \, Tr(M S^\nu M^\dagger S^\mu) \quad .$$

The concept of the density matrix that has been introduced through this simple example can, in the general case, be defined for a particle with spin s scattering on a particle with spin s_t. An arbitrary spin state of the composite system of the nth pair of particles (one in the beam and one in the target) may be described by a vector with components ψ_{nj}. This vector can be represented as a linear combination of the $(2s+1)(2s_t+1)$ basic states of the spin system. For two spin-1/2 protons one could choose as a basis the four states of

$$\xi_1 \propto \uparrow_1\uparrow_2$$

$$\xi_2 \propto \uparrow_1\downarrow_2$$

$$\xi_3 \propto \downarrow_1\uparrow_2$$

$$\xi_4 \propto \downarrow_1\downarrow_2$$

and then $\psi_n = \sum_j \psi_{nj}\,\xi_j$. The arrows represent a quantum state with the spin "up" or "down" in the usual sense and 1, 2 represent the first and second protons respectively. An arbitrary operator in this vector space can also be represented as a linear combination of a complete set of Hermitian matrices S^μ, none of which are linear combinations of each other. The S^μ have the property that $\mathrm{Tr}(S^\mu S^\nu) = (2s+1)(2s_t+1)\delta_{\mu\nu}$. For the vector basis chosen above, the following sixteen matrices constitute

$$S^\mu : \quad 1_1 1_2 \,,\; 1_1\sigma_{2k} \,,\; \sigma_{1j}1_2 \,,\; \sigma_{1j}\sigma_{2k}$$

where 1 is the unit matrix, σ_j are the Pauli matrices, and j, k run from 1 to 3. The expectation value of one of the operators S^μ taken in the spin state of the nth pair of beam and target particles is found in the usual way as

$$\langle S^\mu \rangle_n = \frac{\sum_k \sum_j \psi^*_{nk} S^\mu_{kj} \psi_{nj}}{\sum_j \psi^*_{nj} \psi_{nj}}$$

Experimentally one measures averages over all the beam-target particle pairs, and one calculates the expectation value averaged over the pairs, S^μ, as

$$\langle S^\mu \rangle = \frac{\sum_n \left(\sum_j \psi^*_{nj} \psi_{nj} \right) \langle S^\mu \rangle_n}{\sum_n \left(\sum_j \psi^*_{nj} \psi_{nj} \right)} \qquad \text{(II-1)}$$

and substituting the results of Eq. (II-1) for $\left(\sum_j \psi^*_{nj} \psi_{nj} \right) \langle S^\mu \rangle_n$ one has

$$\langle S^\mu \rangle = \frac{\sum_n \sum_k \sum_j \psi_{nj} \psi^*_{nk} S^\mu_{kj}}{\sum_n \sum_j \psi^*_{nj} \psi_{nj}} \quad . \qquad \text{(II-2)}$$

With the implication that the average over the particle pairs is taken first, the density matrix is defined by

$$\rho_{jk} \equiv \sum_n \psi_{nj} \psi^*_{nk} \quad . \qquad \text{(II-3)}$$

Upon reflection one can see that this density matrix is equivalent to the one introduced through our early example. Using this definition, we can rewrite Eq. (II-2) as

$$\langle S^\mu \rangle = \frac{Tr(\rho S^\mu)}{Tr(\rho)} \quad . \qquad \text{(II-4)}$$

The density matrix, as in our example, can always be expanded as a linear combination of the independent matrices

$$\rho = \sum_\mu a_\mu S^\mu \quad , \qquad \text{(II-5)}$$

where $(2S+1)(2S_t+1) a_\mu = Tr(\rho S^\mu)$.

The density matrix before scattering ρ_i is thus

$$\rho_i = \frac{Tr(\rho_i)}{(2S+1)(2S_t+1)} \sum_\mu \langle S^\mu \rangle_i S^\mu \quad .$$

The density matrix after scattering is found, in the same manner as in our example, to be given by

$$\rho_f = M \rho_i M^\dagger \quad .$$

One can again relate the average expectation values after scattering to the average expectation values before scattering through the equations $\langle S^\mu \rangle_f = Tr(\rho_f S^\mu) / Tr(\rho_f)$,

$$I \langle S^\mu \rangle_f = \frac{1}{(2S+1)(2S_t+1)} \sum_\nu \langle S^\nu \rangle_i Tr(M S^\nu M^\dagger S^\mu) \quad . \tag{II-6}$$

From an experimental standpoint, this equation is most useful because one frequently knows the state of polarization of the beam-target system before scattering and one measures, after the scattering, average expectation values of the spin operators. In the experiment described in this dissertation, an unpolarized beam of protons was scattered on polarized protons in a target. An array of scintillation counters detected counts that were proportional to the differential cross section for elastic p-p scattering. We can use Eq. (II-6) to obtain an expression for this differential cross section I. We take for the set S^μ the 16 operators previously chosen. Before the scatterings occurred, the only nonzero expectation values were

$$\langle 1, 1_2 \rangle = 1$$

$$\langle 1, \underline{\sigma} \cdot \underline{N} \rangle = P \quad ,$$

where $\underline{\sigma}$ is a vector defined as $(\sigma_1 \sigma_2 \sigma_3)$. We have chosen as a coordinate system the three mutually orthonormal vectors,

$$\underline{K} = \frac{\underline{k} - \underline{k}'}{|\underline{k} - \underline{k}'|} \quad , \quad \underline{P} = \frac{\underline{k} + \underline{k}'}{|\underline{k} + \underline{k}'|} \quad , \quad \underline{N} = \frac{\underline{k} \times \underline{k}'}{|\underline{k} \times \underline{k}'|}$$

where $\underline{k}$ is the incident momentum and $\underline{k}'$ the scattered momentum, both in the center-of-mass system. Since our target polarization is always parallel to $\underline{N}$, the normal to the scattering plane, we denote the polarization by the

number p, which is the component of the polarization in the $\underline{N}$ direction. Equation (II-6) then gives us an expression for the average expectation values after the scattering as

$$I\langle S^{\mu}\rangle_f = \tfrac{1}{4}\,\mathrm{Tr}(S^{\mu} M M^{\dagger}) + \tfrac{1}{4} p \underline{N}\cdot \mathrm{Tr}(M \underline{\sigma}_2 M^{\dagger} S^{\mu}) \qquad \text{(II-6')}$$

where $s = s_t = 1/2$ has been used.

After the interaction, all protons from elastic-scattering events were counted regardless of their spin orientation. This, in the notation of our formalism, is equivalent to having measured the average expectation value of the unit operator, $1_1 1_2$, in the final state. Thus from Eq. (II-6'),

$$I = \tfrac{1}{4}\,\mathrm{Tr}(M M^{\dagger}) + \tfrac{1}{4} p \underline{N}\cdot \mathrm{Tr}(M \underline{\sigma}_2 M^{\dagger}) \quad . \qquad \text{(II-7)}$$

The two terms of Eq. (II-7) can be interpreted in the following manner: If both initial beam and target were unpolarized,

$$\rho_i = \frac{1}{(2s+1)(2s_t+1)} \sum_{\mu} \langle S^{\mu}\rangle_i S^{\mu} = \tfrac{1}{4}\langle 1_1 1_2\rangle 1_1 1_2$$

$$\rho_i = \tfrac{1}{4} 1_1 1_2$$

and $$\rho_f = M \rho_i M^{\dagger} = \tfrac{1}{4} M M^{\dagger} \quad ,$$

the unpolarized differential cross section I_0 becomes

$$I_0 = \frac{\mathrm{Tr}(\rho_f)}{\mathrm{Tr}(\rho_i)} = \tfrac{1}{4}\,\mathrm{Tr}(M M^{\dagger}) \quad . \qquad \text{(II-8)}$$

Thus if we define the parameter $P(\theta)$ by the expression,

$$I_0 P(\theta) \equiv \tfrac{1}{4}\,\mathrm{Tr}(M \underline{N}\cdot\underline{\sigma}_2 M^{\dagger}) = \tfrac{1}{4}\,\underline{N}\cdot\mathrm{Tr}(M \underline{\sigma}_2 M^{\dagger}) \quad , \qquad \text{(II-9)}$$

we can write Eq. (II-7) as

$$I = I_0(1 + p P(\theta)) \quad , \qquad \text{(II-10)}$$

where θ is the c.m. scattering angle. (Remember that the target polarization p is either a positive or a negative number, depending upon whether the alignment of the target protons is predominantly parallel or antiparallel to $\underline{N}$.)

The theoretical form of M can be restricted by the requirement of its invariance under spatial rotations, spatial inversions, and time reversal, because the corresponding conservation laws are expected to hold for strong interactions. If M is required to be a scalar or pseudoscalar, the interaction will yield identical results for all observers whose coordinate systems can be connected by pure rotations. A parity transformation inverts the coordinate system, so that a point that was reached by the position vector $r = (x, y, z)$ will be reached by the position vector whose components are $(-x, -y, -z)$. This procedure changes the sign of components of vectors, such as linear momentum; maintains the sign of components of pseudovectors, such as spin; and changes the sign of pseudoscalars and leaves scalars unchanged. Thus if M is constructed as a scalar, it will be invariant under spatial rotations and inversions. The assumption of rotational invariance has also implied that there be no preferred spatial directions in the center-of-mass system other than the incident and final momenta, $\underline{k}$ and $\underline{k}'$, and the particle spins, $\underline{\sigma}_1$ and $\underline{\sigma}_2$. We are thus restricted to combinations of these four vectors in forming M. The terms in M will be at most linear in each σ since M can be represented as a linear sum of the basis matrices:

$$M = A\, 1_1 1_2 + \underline{B} \cdot (\underline{\sigma}_1 1_2) + \underline{C} \cdot (1_1 \underline{\sigma}_2) + (\underline{D} \cdot \underline{\sigma}_1)(\underline{D}' \cdot \underline{\sigma}_2) \quad .$$

The x, y, z axes must be defined in terms of the physical vectors $\underline{k}$ and $\underline{k}'$; and for this purpose we take the previously chosen unit orthogonal vectors $\underline{K}$, $\underline{P}$, $\underline{N}$ in the directions $\underline{k} - \underline{k}'$, $\underline{k} + \underline{k}'$, $\underline{k} \times \underline{k}'$. The following expression is thus the most general form of M invariant under space rotations and inversions:

$$M(\underline{k},\underline{k}') = a + b(\underline{\sigma}_1\cdot\underline{N} - \underline{\sigma}_2\cdot\underline{N}) + c(\underline{\sigma}_1\cdot\underline{N} + \underline{\sigma}_2\cdot\underline{N}) + m(\underline{\sigma}_1\cdot\underline{N}\,\underline{\sigma}_2\cdot\underline{N}) + g(\underline{\sigma}_1\cdot\underline{P}\,\underline{\sigma}_2\cdot\underline{P} + \underline{\sigma}_1\cdot\underline{K}\,\underline{\sigma}_2\cdot\underline{K}) + h(\underline{\sigma}_1\cdot\underline{P}\,\underline{\sigma}_2\cdot\underline{P} - \underline{\sigma}_1\cdot\underline{K}\,\underline{\sigma}_2\cdot\underline{K}) + j(\underline{\sigma}_1\cdot\underline{P}\,\underline{\sigma}_2\cdot\underline{K}) + \ell(\underline{\sigma}_1\cdot\underline{K}\,\underline{\sigma}_2\cdot\underline{P}) \qquad \text{(II-11)}$$

where $a, b, \cdots, \ell$ are scalar functions of the vectors $\underline{k}$ and $\underline{k}'$.

The time-reversal transformation generates a transformed state under the replacement of the time t by -t. Invariance under time reversal is the assertion that a system can develop backwards in time in the same way it normally does forward in time. The effect of this transformation upon the linear- and angular-momentum operators can be summarized by the substitutions $\underline{k} \leftrightarrow -\underline{k}'$ and $\underline{\sigma} \leftrightarrow -\underline{\sigma}$. For M to be invariant under time reversal, none of its terms must change sign with these substitutions. We note for $\underline{k} \to -\underline{k}'$ and $\underline{k}' \to -\underline{k}$ that $\underline{N} \to -\underline{N}$, $\underline{P} \to -\underline{P}$, and $\underline{K} \to \underline{K}$. The coefficients $a, \cdots, \ell$ cannot change sign under time reversal since they are composed of combinations of k^2, k'^2 and $\underline{k}\cdot\underline{k}'$. Thus the terms $j(\underline{\sigma}_1\cdot\underline{P}\,\underline{\sigma}_2\cdot\underline{K})$ and $\ell(\underline{\sigma}_1\cdot\underline{K}\,\underline{\sigma}_2\cdot\underline{P})$ change sign under time reversal and must be equal to zero.

The indistinguishability of the protons is taken into account by the requirement that the interaction matrix M be symmetric under the interchange of the two particles. Thus the term $b(\underline{\sigma}_1\cdot\underline{N} - \underline{\sigma}_2\cdot\underline{N})$ must be equal to zero.* The M matrix that is invariant under rotations, inversion, and time reversal, and symmetric under interchange of the two particles can thus be written as

$$M(\underline{k},\underline{k}') = a + c(\underline{\sigma}_1\cdot\underline{N} + \underline{\sigma}_2\cdot\underline{N}) + m(\underline{\sigma}_1\cdot\underline{N}\,\underline{\sigma}_2\cdot\underline{N}) + g(\underline{\sigma}_1\cdot\underline{P}\,\underline{\sigma}_2\cdot\underline{P} + \underline{\sigma}_1\cdot\underline{K}\,\underline{\sigma}_2\cdot\underline{K}) + h(\underline{\sigma}_1\cdot\underline{P}\,\underline{\sigma}_2\cdot\underline{P} - \underline{\sigma}_1\cdot\underline{K}\,\underline{\sigma}_2\cdot\underline{K}). \qquad \text{(II-12)}$$

If one uses the form of $M(\underline{k},\underline{k}')$ given in Eq. (II-12) and evaluates Eq. (II-9), which was used to define $P(\theta)$, one can obtain

*Since the protons are identical fermions, the total wave function must be antisymmetric. In the signlet-triplet notation, the operator $(\underline{\sigma}_1 - \underline{\sigma}_2)\cdot\underline{N}$ changes the spin state of the system from triplet to singlet or vice versa. It must therefore also change the angular momentum ℓ, since $J = \ell + S$ must be conserved. But changing ℓ by one is not allowed by parity conservation. Hence the term is zero.

$$P(\theta) = \frac{Tr\,(M\,\underline{N}\cdot\underline{\sigma}_2\,M^\dagger)}{Tr(M M^\dagger)}$$

$$P(\theta) = \frac{(ac^* + a^*c) + (cm^* + c^*m)}{aa^* + 2cc^* + mm^* + gg^* + hh^*} \qquad \text{(II-13)}$$

The original double-scattering experiments, which were performed to measure polarization, involved the measurement of an asymmetry ϵ given by

$$\epsilon = P_A P_B = \frac{Tr(M_A M_A^\dagger\,\underline{N}\cdot\underline{\sigma}_1)}{Tr(M_A M_A^\dagger)} \frac{Tr(M_B\,\underline{N}\cdot\underline{\sigma}_1\,M_B^\dagger)}{Tr(M_B M_B^\dagger)} \qquad \text{(II-14)}$$

where the subscripts A and B refer to the first and second targets, respectively. The conventional definition of the polarization parameter is $P(\theta) = Tr(\rho_f\,\underline{N}\cdot\underline{\sigma}_1)/Tr(\rho_f)$. At target A this can be written

$$P_A = \frac{Tr\,(M_A\,M_A^\dagger\,\underline{N}\cdot\underline{\sigma}_1)}{Tr\,(M_A M_A^\dagger)}$$

Notice then that $P(\theta)$, according to its usual definition, is the polarization of the scattered particles that results when an unpolarized beam is scattered by an unpolarized target. In the double-scattering experiments the polarization induced by the first scattering produced an asymmetry in the second scattering. The analyzing power -- the extent to which beam polarization at the second target produces asymmetry -- is defined, then, as $P_B = Tr\,(M_B\,\underline{N}\cdot\underline{\sigma}_1\,M_B^\dagger)/Tr\,(M_B\,M_B^\dagger)$. For the case of elastic proton-proton scattering where $M_A = M_B = M$ [which has the form given in Eq. (II-12)], we will show that the two factors are equal, $P_A = P_B$. This is the basis for the usual statement that polarizing power is equal to the analyzing power. One can see, then, that the $P(\theta)$ defined by Eq. (II-9) is the usual polarization parameter for elastic p-p scattering. One should note that although $\underline{\sigma}_1$ occurs in the double scattering experiment (since one usually

speaks of the beam particles here) and $\underline{\sigma}_2$ occurs in the polarized-target experiment (since the target particle is polarized), the M matrix has been made symmetric with respect to the first and second particles because of the identity of the two protons. This insures that results of identical procedures that use $\underline{\sigma}_1$ or $\underline{\sigma}_2$ will be equivalent. Confusion about the bookkeeping notation will be avoided if one remembers that the polarization parameter must be an antisymmetric function about 90° in the c.m. system. The proof that $Tr(MM^{\dagger}\underline{N}\cdot\underline{\sigma}) = Tr(M\,\underline{N}\cdot\underline{\sigma}\,M^{\dagger})$ is not entirely trivial since neither $\underline{N}\cdot\underline{\sigma}_1$ nor $\underline{N}\cdot\underline{\sigma}_2$ commutes with M, but the proof does follow by straightforward algebra and with the trace taken as indicated. One uses the following properties of the ~~Dirac~~ Pauli σ matrices

$$\sigma_\ell \sigma_j = \delta_{\ell j} + i\,\epsilon_{\ell jk}\,\sigma_k$$

$$\sigma_\ell^{\dagger} = \sigma_\ell$$

$$Tr\,\sigma_\ell = 0 \quad ,$$

where ℓ, j, k run from 1 to 3 and

$$\delta_{\ell j} = \begin{cases} 1 & \text{for } \ell = j \\ 0 & \text{for } \ell \neq j \end{cases}$$

$$\epsilon_{\ell jk} = \begin{cases} +1 & \text{for } \ell jk = 123 \text{ or any cyclic permutation thereof} \\ -1 & \text{for } \ell jk = 213 \text{ or any cyclic permutation thereof} \\ 0 & \text{for } \ell = j \text{ or } \ell = k \text{ or } j = k \end{cases} ,$$

and σ_ℓ belonging to different spin spaces commute (i.e., $\sigma_{1\ell}\,\sigma_{2j} = \sigma_{2j}\,\sigma_{1\ell}$). With the previous coordinate system, the Pauli matrices can be written as

$$\sigma_{1\ell} \begin{cases} \sigma_{1K} \equiv \underline{K}\cdot\underline{\sigma}_1 \\ \sigma_{1P} \equiv \underline{P}\cdot\underline{\sigma}_1 \\ \sigma_{1N} \equiv \underline{N}\cdot\underline{\sigma}_1 \end{cases}$$

$$\sigma_{2j} \begin{cases} \sigma_{2K} \equiv \underline{K}\cdot\underline{\sigma}_2 \\ \sigma_{2P} \equiv \underline{P}\cdot\underline{\sigma}_2 \\ \sigma_{2N} \equiv \underline{N}\cdot\underline{\sigma}_2 \end{cases}$$

With this notation,

$$M = a + c(\sigma_{1N} + \sigma_{2N}) + m(\sigma_{1N}\sigma_{2N}) + d(\sigma_{1P}\sigma_{2P}) + f(\sigma_{1K}\sigma_{2K})$$

$$M^\dagger = a^* + c^*(\sigma_{1N} + \sigma_{2N}) + m^*(\sigma_{1N}\sigma_{2N}) + d^*(\sigma_{1P}\sigma_{2P}) + f^*(\sigma_{1K}\sigma_{2K})$$

where * denotes the complex conjugate and

$$d \equiv g + h$$

$$f \equiv g - h .$$

Thus

$$\begin{aligned} MM^\dagger = \{ & aa^* + ca^*(\sigma_{1N} + \sigma_{2N}) + ma^*\sigma_{1N}\sigma_{2N} + da^*\sigma_{1P}\sigma_{2P} + fa^*\sigma_{1K}\sigma_{2K} \\ & + ac^*(\sigma_{1N} + \sigma_{2N}) + 2cc^*(1 + \sigma_{1N}\sigma_{2N}) + mc^*(\sigma_{2N} + \sigma_{1N}) \\ & + idc^*(\sigma_{1K}\sigma_{2P} + \sigma_{1P}\sigma_{2K}) - ifc^*(\sigma_{1P}\sigma_{2K} + \sigma_{1K}\sigma_{2P}) \\ & + am^*\sigma_{1N}\sigma_{2N} + cm^*(\sigma_{1N} + \sigma_{2N}) + mm^* \\ & - dm^*\sigma_{1K}\sigma_{2K} - fm^*\sigma_{1P}\sigma_{2P} + ad^*\sigma_{1P}\sigma_{2P} \\ & - icd^*(\sigma_{1K}\sigma_{2P} + \sigma_{1P}\sigma_{2K}) - md^*\sigma_{1K}\sigma_{2K} \\ & + dd^* - fd^*\sigma_{1N}\sigma_{2N} + af^*\sigma_{1K}\sigma_{2K} \\ & + icf^*(\sigma_{1P}\sigma_{2K} + \sigma_{1K}\sigma_{2P}) - mf^*\sigma_{1P}\sigma_{2P} \\ & - df^*\sigma_{1N}\sigma_{2N} + ff^* \} . \end{aligned}$$

When the trace is taken,

$$I_0 = \mathrm{Tr}\, MM^\dagger = aa^* + 2cc^* + mm^* + dd^* + ff^*$$

(We have assumed that the initial density matrix is normalized to unity when we set $I_0 = \mathrm{Tr}(MM^\dagger)$. One then easily obtains

$$\mathrm{Tr}(MM^\dagger\sigma_{1N}) = (ac^* + a^*c + cm^* + c^*m) .$$

Next one writes out

$$
\begin{aligned}
M\sigma_{iN}M^{\dagger} = \{ & a a^{*}\sigma_{iN} + c a^{*}(1 + \sigma_{iN}\sigma_{2N}) + m a^{*}\sigma_{2N} \\
& + i d a^{*}\sigma_{iK}\sigma_{2P} - i f a^{*}\sigma_{iP}\sigma_{2K} + a c^{*} \\
& + c c^{*}(\sigma_{iN} + \sigma_{2N}) + m c^{*}\sigma_{iN}\sigma_{2N} + d c^{*}\sigma_{iP}\sigma_{2P} \\
& + f c^{*}\sigma_{iK}\sigma_{2K} + a c^{*}\sigma_{iN}\sigma_{2N} + c c^{*}(\sigma_{iN} + \sigma_{2N}) \\
& + m c^{*} - d c^{*}\sigma_{iK}\sigma_{2K} - f c^{*}\sigma_{iP}\sigma_{2P} + a m^{*}\sigma_{2N} \\
& + c m^{*}(\sigma_{iN}\sigma_{2N} + 1) + m m^{*}\sigma_{iN} \\
& + i d m^{*}\sigma_{iP}\sigma_{2K} - i f m^{*}\sigma_{iK}\sigma_{2P} - i a d^{*}\sigma_{iK}\sigma_{2P} \\
& + c d^{*}(\sigma_{iP}\sigma_{2P} - \sigma_{iK}\sigma_{2K}) - i m d^{*}\sigma_{iP}\sigma_{2K} \\
& - d d^{*}\sigma_{iN} + f d^{*}\sigma_{2N} + i a f^{*}\sigma_{iP}\sigma_{2K} \\
& - c f^{*}(-\sigma_{iK}\sigma_{2K} + \sigma_{iP}\sigma_{2P}) + i m f^{*}\sigma_{iK}\sigma_{2P} \\
& + d f^{*}\sigma_{2N} - f f^{*}\sigma_{iN} \}
\end{aligned}
$$

and taking the trace, we obtain

$$
Tr(MM^{\dagger}\sigma_{iN}) = (a c^{*} + a^{*} c + c m^{*} + c^{*} m) \quad .
$$

Thus

$$
Tr(M\sigma_{iN}M^{\dagger}) = Tr(MM^{\dagger}\sigma_{iN}) \quad .
$$

Remembering that M is symmetric in $\underline{\sigma}_1$ and $\underline{\sigma}_2$, one can show in a similar fashion that $Tr(M\sigma_{2N}M^\dagger) = Tr(M\sigma_{1N}M^\dagger) = I_0 P(\theta)$. The polarization parameter $P(\theta)$ measured with the polarized target is thus the same as that measured in the double-scattering experiments.

It is worth noting that if M were not required to be invariant under time reversal and the form of M given in Eq. (II-11) were used, the polarizing power and the analyzing power would no longer be equal. In fact one would have obtained the following expressions:

$$Tr(MM^\dagger\sigma_{1N}) = \{(ac^* + a^*c) + (cm^* + c^*m) + i(fg^* - f^*g) - i(dl^* - d^*l)\}$$

$$Tr(M\sigma_{1N}M^\dagger) = \{(ac^* + a^*c) + (cm^* + c^*m) - i(fg^* - f^*g) + i(dl^* - d^*l)\}.$$

The presentation in this section is nonrelativistic. In the energy region with which this dissertation is concerned, it is necessary to use the relativistic kinematics. Stapp has given the relativistic treatment of the interaction matrix M.[6] It turns out that for polarization measurements, the results of the relativistic treatment are indentical to that from the nonrelativistic treatment. The reason this is so depends upon the fact that spin components perpendicular to the direction of the motion of the particle are unaffected by Lorentz transformations. For the polarization measurements described here, the nonrelativistic formalism is sufficient.

III. BEAM

The Berkeley 184-inch synchrocyclotron accelerated protons to a fixed energy. Various thicknesses of an absorber were used to degrade this maximum energy to lower energies. The manner in which the proton beam was formed makes it unlikely that it had any significant degree of polarization. In addition, the symmetry of the arrangement prohibited introducing any polarization that had a component perpendicular to the plane of the scattering. Figure 1 shows a diagram of the beam system.

After a spin-independent injection and acceleration, the protons entered an auxiliary dee that could be used to stretch the beam spill to as much as 12 msec out of 16.7 msec of the acceleration cycle. The beam was extracted from the main magnetic field by the well-known Tuck-Ting method. The cyclotron had provision for inserting up to 10 inches of Cu absorber in the external beam. To obtain the following beams we used the indicated thicknesses.

Energy (MeV)	Thickness of Cu absorber (in.)
740±4	0
683±6	1 1/2
619±4	3 1/16
334±5	9 5/8

Following this was a premagnet collimator whose aperture could be adjusted.

The cyclotron steering magnet, which is a bending magnet with a 6-inch gap, then deflected the beam in the horizontal plane through an angle of 18° into two 8-inch-aperture quadrupoles. These quadrupoles were used as a doublet to focus a 2-inch-diameter spot upon a collimator placed in the proton cave. The size of this collimator could be varied from 2 by 2 inches to 1/8 by 1/8 inch. The jaws of the collimator consisted of 8 inches of copper in the beam direction. This provided rectangular sources for an 8-inch-aperture quadrupole (used

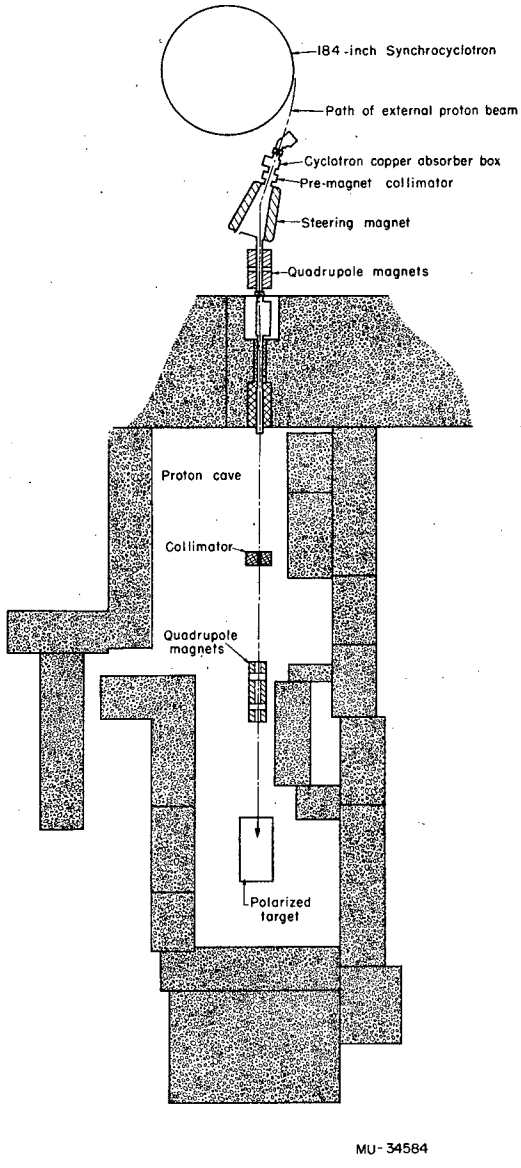

Fig. 1. Proton-beam-transport system.

as a triplet) to focus the beam upon the crystals of the polarized target. The plane of the scattering was vertical. To minimize spreading of the beam (due to multiple Coulomb scattering) as it passed through the proton cave, a helium bag was used. The helium bag consisted of a plastic bag filled with 1 atmosphere of helium gas and extended most of the length of the cave from the collimator to the polarized target.

Since only one bending of the beam occurred, there existed an energy distribution spread linearly across the target. But this was in the horizontal plane and perpendicular to the plane of the scattering. The energies of the beams were measured by a range telescope. Figure 2 shows the counter arrangement of the range telescope and the electronics.

Coincidences $S_1 S_4$ were counted to normalize the points of the range curve. Coincidences $S_1 S_4 S_2$ were counted to provide an integral range curve, and coincidences $S_1 S_4 S_2$ with S_3 in anti-coincidence provided a differential range curve. Measurements of beam energy were made with three choices of copper in the cyclotron copper absorber box (0, 3 1/16, and 9 5/8 inches). The intensity of the external proton beam was made as low as possible and still be compatible with control of the intensity to within a factor of two. Varying amounts of Cu absorber pieces calibrated in g/cm^2 were inserted between S_1 and S_2, and the range curves were taken. Figure 3 shows the curve taken with no Cu absorber in the cyclotron absorber box. The range in Cu was found from both the differential and integral range curves. To these values was added, as was appropriate, the Cu equivalent of the scintillators and one-half the thickness of the differential Cu slab. Range energy tables from Rich and Madey were then used to determine the energies.[7]

To obtain the range curve with no copper absorber in the cyclotron box, 7 inches of copper was placed before counter S_4. This served to reduce the singles rates in the counters and was included in the range calculations. The Cu absorber pieces in the cyclotron box were not accessible for calibration. With the nominal thickness of the copper in inches and an assumed density of 8.94 g/cm^3, the

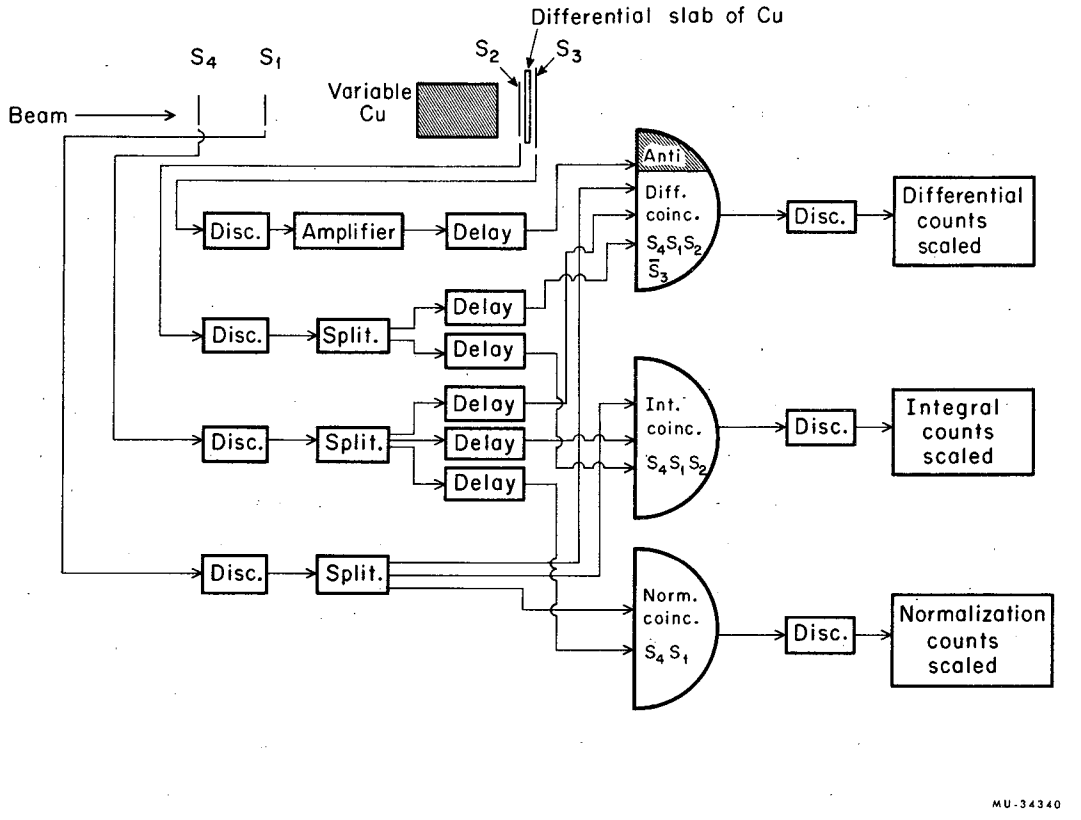

Fig. 2. Range counter-telescope with associated electronics. Counter dimensions were:

S_4 1×1×1/4 in.
S_1 1×1×1/4 in.
S_2 6-in. diam circle ×1/4 in. thick
S_3 7×8×1/2 in.

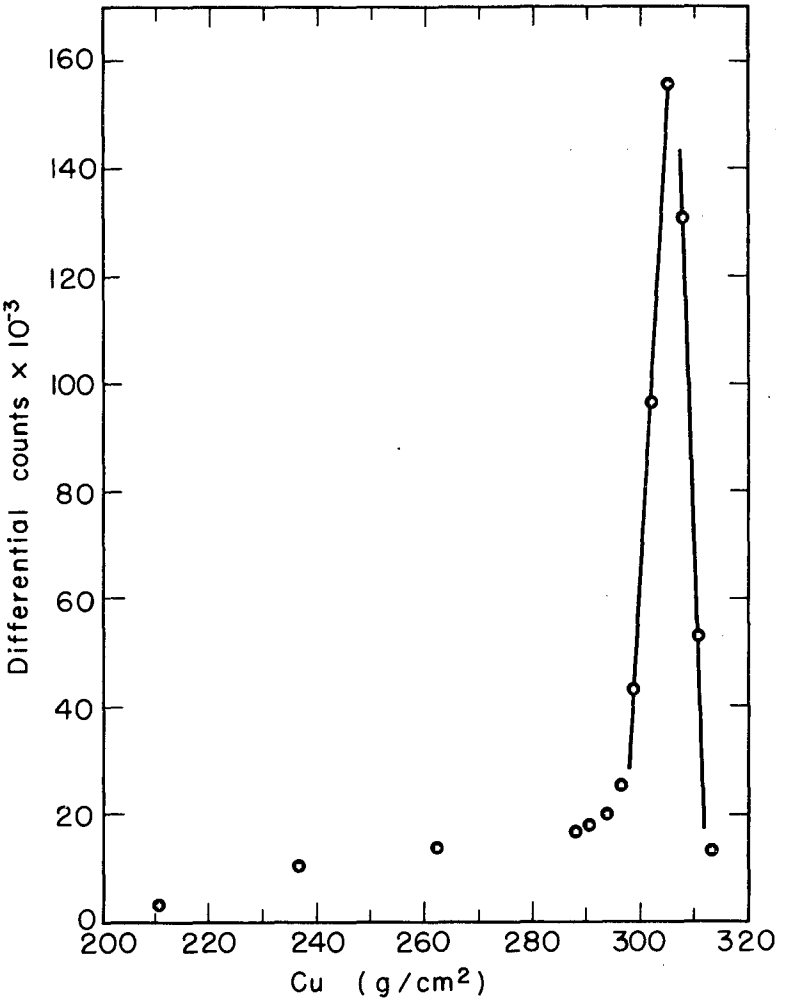

Fig. 3. Differential range curve of full-energy beam (i.e., no copper absorber in the cyclotron copper absorber box). Range in copper = 308.9± 2.5 g/cm^2 (305.2 g/cm^2 center of differential curve at half height + 3.7 g/cm^2 for copper equivalent of S_4, S_1, 1/2 S_2, and one-half differential slab). This corresponds to 740± 4 MeV.

values of CuBOX + CuRANGE for the three curves are listed in Table I. The total thickness CuBOX + CuRANGE in each case must add to the same value because the sychrocyclotron is a fixed-energy machine. Since the values agree, within the accuracy of the measurements, we assumed this density and calculated the energy of 683 MeV from the value found for the full-energy beam (308.9 g/cm^2). The results given include the calculated energy loss to the center of the target:

736±5 MeV

679±7 MeV

614±5 MeV

328±6 MeV

At energies 736, 679, and 328 MeV, the beam spots at the target were from 1.5 to 2 times the area of the target. At 614 MeV, the beam spot was approximately the size of the target. Effect of the size of the beam spot on the measurement of $P(\theta)$ is discussed in Sec. IX.

Table I. Results of range-energy measurements.

Thickness of Cu in cyclotron box (nominal inches)	CuBOX ≡ Cu in cyclotron box for a copper density=8.94 g/cm^3 (g/cm^2)	CuRANGE ≡ range in Cu measured with range telescope (g/cm^2)	CuBOX + CuRANGE (g/cm^2)	Energy (MeV)
0	0.0	308.9±2.5	308.9±2.5	740±4
3 1/16	69.5	237.4±2.5	306.9±2.5	619±4
9 5/8	238.3	90.9±2.5	309.5±2.5	334±5

The energy spread of each beam was 15 MeV full width at half maximum.

IV. TARGET

The polarized target used in the experiment has been described in detail by Schultz.[8] Only a brief summary is given here.

The target itself consists of four single crystals of $La_2Mg_3(NO_3)_{12}\cdot 24\ H_2O$. A small fraction of the La ions have been replaced with the paramagnetic ions of Nd^{142}, and the hydrogen nuclei in the waters of hydration are polarized by means of a technique called dynamic nuclear orientation.[9] The hydrogen nuclei provide a polarized proton target with an equivalent thickness of 0.15 g/cm^2.

The crystals are cooled in a liquid helium bath whose temperature has been lowered to about 1.2°K by decreasing the vapor pressure of the helium with a mechanical pump. An external magnetic field of 18.75 kG applied to the crystals splits the two spin states of the spin-1/2 protons. The polarization of the target is defined as the fractional difference in the population densities of these spin states:

$$P = \frac{N(+1/2) - N(-1/2)}{N(+1/2) + N(-1/2)} \quad . \qquad \text{(IV-1)}$$

At this temperature and field the Boltzman distributions in the two energy states provide a "natural" polarization of 0.16%. To attain higher polarizations of either sign, the crystals are irradiated with microwaves of frequencies near the electron resonance (71 kMC for 18.75 kG). The paramagnetic Nd^{142} ions at this temperature behave like spin-1/2 electrons with an effective g factor of 2.70. These ions can be thought of as unpaired electrons whose spins couple with the spins of neighboring protons of the hydrogen nuclei. Figure 4 shows an energy-level diagram for an electron and proton spin system in an external magnetic field. In Fig. 4, $\Delta = g_e \mu_e H_0$ and $\delta = g_p \mu_n H_0$ where μ_0 and μ_n are the Bohr magneton and the nuclear magneton, H_0 is the external magnetic field, g_e and g_p are the spectroscopic splitting factors for the electron and proton respectively.* k is the Boltzman constant; and T is the absolute temperature. Saturation of one of the forbidden transitions, which involves a simultaneous flip

*M, m denote magnetic quantum numbers of the electron and proton.

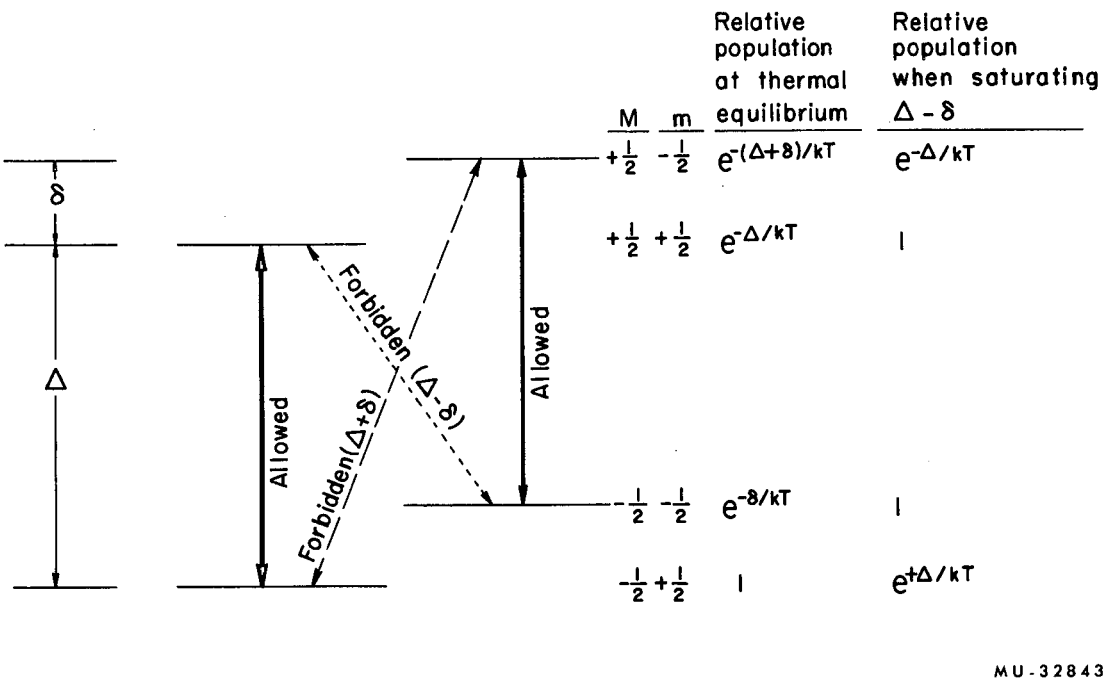

Fig. 4. Energy levels of an electron and a proton spin in an external magnetic field, showing magnetic quantum numbers of the four states and relative populations at thermal equilibrium and when saturating the partially forbidden transition at frequency $(\Delta-\delta)/\hbar$.

of an electron and proton spin, with the appropriate microwave frequency produces the indicated relative population densities of the spin states. It is important that the relaxation time for the "electron" spin flip is much less than the relaxation time for the proton spin flip. For the present target the relaxation time for the electron spin flip is of the order of milliseconds, whereas that of the proton spin flip is about 15 minutes. Thus each neodymium ion can successively flip many neighboring proton spins. Further propagation of the proton polarization outward from the neighborhood of the neodymium center depends on proton-proton spin interactions, which cause mutual flips of neighboring protons. From the definition of the polarization one obtains the "natural" polarization of the protons in thermal equilibrium with the liquid helium bath at temperature T and in the external magnetic field H_0 to be

$$P = \tanh \frac{\mu_p \cdot \underline{H}_0}{2kT} \quad . \qquad (IV-2)$$

When one of the forbidden transitions is saturated, the proton polarization becomes

$$P = \tanh \frac{\mu_e \cdot \underline{H}_0}{2kT} \quad . \qquad (IV-3)$$

Target polarizations as large as 65% have been obtained with the present target.

The determination of the target polarization consists of measuring the frequency and strength of the nuclear magnetic resonance of the protons and the temperature of the liquid helium bath. When the target polarization is unenhanced and at thermal equilibrium with the helium bath, the strength of the nuclear magnetic resonance (NMR) signal is recorded and the temperature measured. The "natural" polarization under these conditions is computed from the frequency of the resonance and the temperature of the bath. This in effect calibrates the recorded thermal equilibrium NMR signal. After the polarization of the target has been enhanced, the NMR signal is continuously monitored and the enhancement of the target polarization

is computed from the ratio of the areas of the enhanced NMR signal to the unenhanced signal. The absolute value of the target polarization is then obtained by multiplying this enhancement ratio by the computed polarization of the unenhanced signal. The actual calculation of the target polarization must take into account the effect of the characteristics of the detection system; this calculation is summarized in Sec. V.

In the scattering experiment the elements in the target, other than hydrogen, generated background events. The detected background events were primarily of two kinds: quasi-elastic scatterings of incident beam protons with bound protons in the nuclei of the nonhydrogen elements; and accidental coincidences between scattered protons from different scatterings occurring within the resolution time of the coincidence circuit. To evaluate the shape of the background, we constructed a dummy target to simulate the crystal target in kinds of atoms and in their respective proportions by weight. At each measured counter position and energy, runs were also made with the dummy target. Attempts were made to keep all other conditions of the experimental setup identical between the set of dummy target runs and the crystal target runs. Table II gives the composition of the dummy target.

Table II. Composition of the dummy target.

Target (26.1 grams of $La_2Mg_3(NO_3)_{12} \cdot 24H_2O$)			
Element	Atomic No.	Atomic weight	Total weight (grams)
La	57	138.9	4.7
Mg	12	24.3	1.3
N	7	14.0	2.9
O	8	16.0	16.4
H	1	1.0	0.8

Dummy target (3.36 grams of MgF_2, 6.70 grams of $BaCO_3$, and 15.65 grams of CF_2:CF_2(Teflon))			
Element	Atomic No.	Atomic weight	Total weight (grams)
Ba	56	137.4	4.7
Mg	12	24.3	1.3
C	6	12.0	4.2
O	8	16.0	1.6
F	9	19.0	14.0
—	—	—	—

V. MEASUREMENT OF THE TARGET POLARIZATION

The polarization of the free protons in the target was measured by monitoring their nuclear magnetic resonance signal. The crystals were positioned in the center of an rf pickup coil that consisted of two rectangular "figure eight" loops. Figure 5 shows a sketch of the crystals and NMR pickup coil. Two crystals were fastened to each side of the aluminum septum used to guide the flux lines into a more uniform rf magnetic-field configuration in the region occupied by the crystals. The leads from the coil were connected in parallel with a variable capacitance, forming an effective parallel capacitance-inductance circuit. A rf-signal generator drove the circuit at resonance. This generator fed the tuned circuit through such a large capacitive reactance x_s that it could be considered as a constant current source. When the frequency of the rf generator passed through the proton resonance value ν_p appropriate to the external magnetic field H_0, the spin systems of the protons absorbed or emitted energy to the rf field (depending upon whether they were aligned predominantly parallel or antiparallel to the field). This appeared in the resonance circuit as a change in the impedance of the circuit. Since the rf generator effectively generated a constant current, this change in impedance was detected by measuring the linearly related voltage change of the circuit. To facilitate the observation of this signal, the external magnetic field was perturbed with a small alternating 400 cps component. This was achieved by a pair of coils (of approximate Helmholtz geometry) wrapped about the pole faces of the target magnet and fed an alternating current of 400 cps. The magnitude of this current was restricted so that the perturbation would not be large enough to disturb the stability of the polarization method. This perturbation of the field manifested itself in the detection system as a 400-cycle amplitude modulation on the rf voltage. The rf voltage across the resonance circuit was amplified and then, by means of a diode, rectified. The diode voltage gave a 400-cycle signal whose amplitude was proportional to the slope of the proton-resonance-absorption curve. This signal was amplified and converted by a lock-in

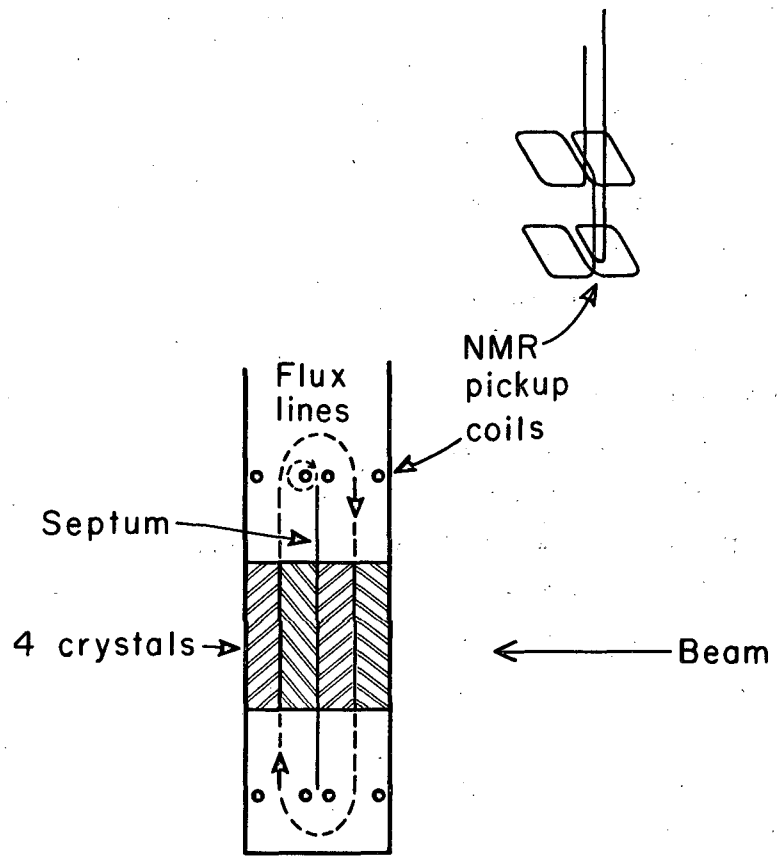

Fig. 5. Sketch of the polarized-target crystals and the NMR pick-up coils. There were four crystals, each of dimension ≈ 1×1×1/4 in.

phase-sensitive detector to a proportional dc signal. This signal, representing the derivative of the NMR line, is called the differential signal. It was recorded on a chart recorder and digitized for recording on paper tape. The dc voltage level of the rf rectifying diode was also recorded and simultaneously, as was the differential signal, digitized and taped. Figure 6 is a schematic of the detection system.

A complex rf susceptibility $X = X' - i X''$ can be defined for the crystals. For a single Lorentz resonance, the dispersive X' and absorptive X'' components can be expressed as[10]

$$X' = -\frac{1}{2} X_0 \omega_0 T_2 \frac{T_2(\omega - \omega_0)}{1 + T_2^2(\omega - \omega_0)^2 + (\gamma H_1)^2 T_1 T_2} \qquad (V-1)$$

$$X'' = \frac{1}{2} X_0 \omega_0 T_2 \frac{1}{1 + T_2^2(\omega - \omega_0)^2 + (\gamma H_1)^2 T_1 T_2},$$

where ω_0 = resonant frequency

T_1 = relaxation time for proton spin component along $\underline{H}_0$

T_2 = relaxation time for proton spin component perpendicular to $\underline{H}_0$

H_1 = component of rf magnetic field perpendicular to the external field $\underline{H}_0$

γ = gyromagnetic ratio of the proton.

The static Curie susceptibility X_0 is

$$X_0^{-1} = \frac{3 k T}{p N_v \gamma^2 I(I+1)} \qquad (V-2)$$

where

I = spin of proton

k = Boltzman constant

T = temperature of crystal

p = polarization of target

N_v = number of protons per unit volume.

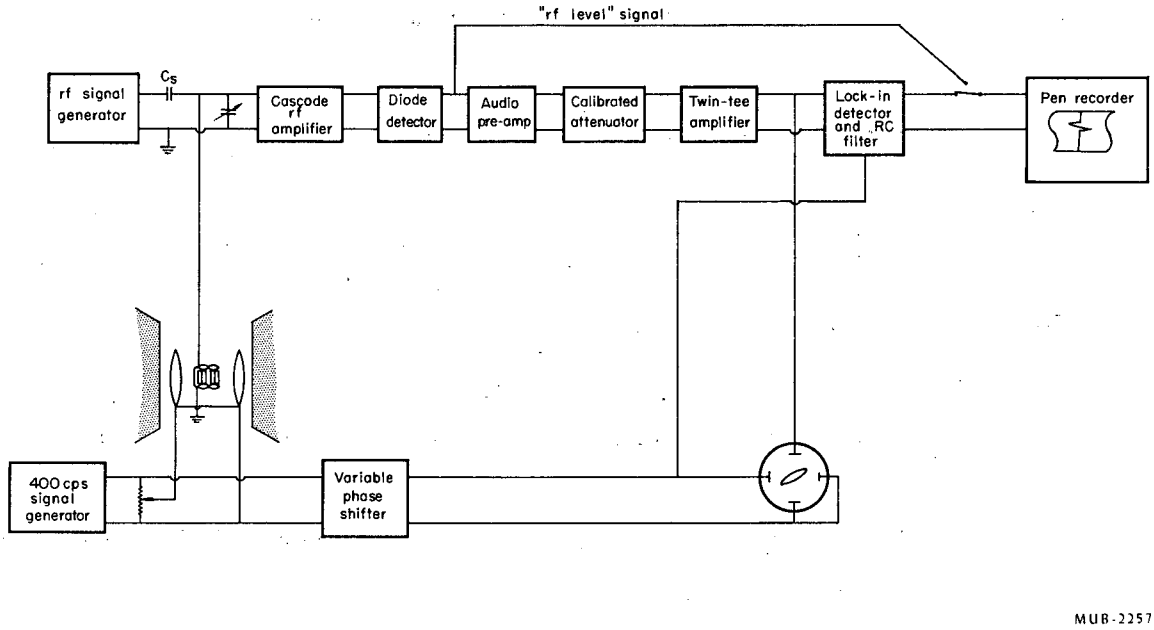

Fig. 6. Schematic of the NMR detection system.

The factor $p N_v$ gives the net difference per unit volume of the number of spins aligned with or against the field, since each of the two states contributes oppositely to X_0. One notes that the complex susceptibility X is proportional to the polarization p. Although the rf susceptibility of the crystal cannot be derived from a single Lorentz shape, it can be thought of as a linear sum of the 48 single-proton resonances in the crystal molecule. A shape factor $g(\omega - \gamma H)$ is introduced to take this into account, such that

$$X \propto p \times g(\omega - \gamma H) . \qquad (V-3)$$

H is the external magnetic field, including the 400-cycle perturbing component. The integral of the complex function $g(\omega - \gamma H)$ over all frequencies is a real constant and is usually normalized to unity. As the magnitude of the target's polarization changes, these line shapes can change because the relative positions of the 48 single-proton resonances (whose frequencies may depend on the spins of the nearest-neighbor protons) shift with respect to each other. However, it is believed that the overall normalization does not change.

The complex impedance Z of the tuned circuit can be written as

$$\frac{1}{Z} = \frac{1}{Z_L} + \frac{1}{Z_c} . \qquad (V-4)$$

where $Z_c = 1/i\,\omega c$, and c is the value of the parallel capacitance. The impedance Z_L is the sum of resistive and inductive impedance of the circuit

$$Z_L = R + i\,\omega\,L\,(1 + 4\,\pi\,\eta X), \qquad (V-5)$$

where L is the inductance of the coil in the absence of resonance absorption and η is the fraction of the volume of the coil occupied by the crystals. Upon differentiating Z_L with respect to the external field, one obtains

$$\frac{\partial Z_L}{\partial(\gamma H)} = \text{constant} \times p \times \frac{\partial g}{\partial(\gamma H)} \quad . \tag{V-6}$$

The detected voltage across the circuit is directly proportional to Z:

$$V = \text{constant} \times \frac{Z_L Z_c}{Z_L + Z_c} \quad . \tag{V-7}$$

The differential signal of V was recorded

$$\frac{\partial V}{\partial(\gamma H)} = \left(\frac{Z_c}{Z_L + Z_c} - \frac{Z_L Z_c}{(Z_L + Z_c)^2} \right) \frac{\partial Z_L}{\partial(\gamma H)} \times \text{constant}$$

$$\frac{\partial V}{\partial(\gamma H)} = \frac{Z_c^2}{(Z_L + Z_c)^2} \frac{\partial Z_L}{\partial(\gamma H)} \times \text{constant} \quad . \tag{V-8}$$

or

$$\frac{\partial V}{\partial(\gamma H)} \propto \frac{|Z|^2}{Z_L^2} \frac{\partial Z_L}{\partial(\gamma H)} \quad .$$

With the assumption that the change in the absolute magnitude of Z_L is small,

$$\frac{\partial Z_L}{\partial(\gamma H)} \propto \frac{1}{|Z|^2} \frac{\partial V}{\partial(\gamma H)}$$

$$\frac{\partial Z_L}{\partial(\gamma H)} \propto \frac{1}{|V|^2} \frac{\partial V}{\partial(\gamma H)} \tag{V-9}$$

and from Eq. (V-6)

$$p \frac{\partial g}{\partial(\gamma H)} \propto \frac{1}{|V|^2} \frac{\partial V}{\partial(\gamma H)}$$

p can be obtained by integration (where $\frac{\partial g}{\partial(\gamma H)} = - \frac{\partial g}{\partial \omega}$ because $g = g(\omega - \gamma H)$)

$$p \times g(\omega' - \gamma H) \propto \int_0^{\omega'} d\omega \frac{1}{|V(\omega)|^2} \frac{\partial V(\omega)}{\partial(\gamma H)}$$

$$p \propto \int_0^{\infty} d\omega' \int_0^{\omega'} d\omega \frac{1}{|V(\omega)|^2} \frac{\partial V(\omega)}{\partial(\gamma H)} \quad . \qquad \text{(V-10)}$$

Thus a double integration, with respect to frequency, of the product of the detected differential signal divided by the square of the dc voltage of the rectifying diode gives a quantity proportional to the polarization of the target. Note that the differential signal actually detected was $\frac{\partial |V|}{\partial(\gamma H)}$ instead of $\frac{\partial V}{\partial(\gamma H)}$, and a correction should be made for this difference. It is estimated that the correction is small,[11] and it has not been made. As is explained later, the differential signal and the dc level voltage were digitized and eventually recorded on magnetic tape. The double integrations of Eq. (V-10) were done numerically on an IBM 7044 computer.

The procedure for measuring the target polarization consisted of recording the NMR proton signal when the crystals were in thermal equilibrium with the liquid He bath and no microwaves were present to stimulate the "forbidden transitions." This signal was called the thermal equilibrium (TE) signal. While such a TE signal was being recorded, the vapor pressure of the liquid He was measured with an oil manometer and the central rf frequency at which the resonance occurred was noted. The vapor pressure is effectively a measure of the temperature of the system, and the central-resonance frequency a measure of the strength of the external field. The absolute magnitude of the target polarization is computed under these conditions from Eq. (IV-1)--

$$p_{TE} = \tanh \frac{\underline{\mu}_p \cdot \underline{H}_0}{2kT} \quad .$$

The corresponding NMR proton signal recorded is subsequently doubly integrated to give an "area" A_{TE}. This area can thus be calibrated in terms of absolute magnitude of polarization:

$$A_{PTE} = \frac{\text{NMR signal area}}{\text{polarization}} = \frac{A_{TE}}{p_{TE}} \quad .$$

Several of these TE signals were measured before and after a set of experimental runs. Their average $\bar{A}_{PTE}$ was computed. During an experimental run, the NMR signal was continuously recorded by an ink-pen paper-chart recorder. A sample signal for each run was usually digitized and recorded on paper tape for later double integration. The "area" A_R of the sample run was divided by $\bar{A}_{PTE}$ to give the absolute magnitude of the polarization p_{ri}, which corresponded to this sample. For a set of experimental runs, the peak-to-peak amplitudes of the differential NMR signals of these samples were plotted against their absolute polarizations. This gave a calibration curve of target polarization versus peak-to-peak amplitude. Figure 7 shows an example of one of the graphs. The average target polarization of an experimental run was then found from the graph according to the average value of the peak-to-peak signals recorded during the length of the run. The accuracy of these measurements is discussed in Sec. IX.

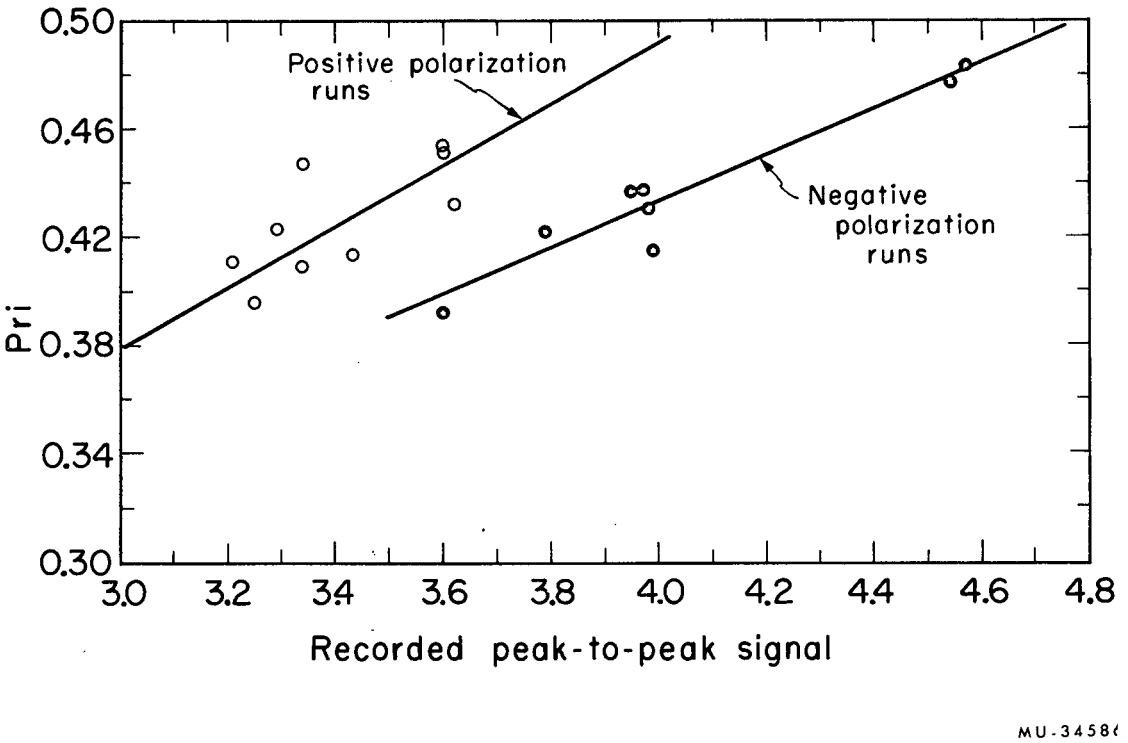

Fig. 7. Calibration curve of target polarization versus peak-to-peak amplitude for runs taken at 736 MeV with the counters covering the angular region from 65.5 to 83.2° center of mass.

VI. COUNTERS

An upper array of 10 scintillation counters and a lower array of 10 scintillation counters were used to detect the elastically scattered protons. A count was stored in a coded bin of a 100-channel analyzer for each event detected. Figure 8 depicts the counter arrangement. Each counter of the upper array measured 2 in. in the plane of scattering, 1 in. perpendicular to the plane, and 1/2-in. in thickness. Each counter of the lower array measured 3/2 in. by 3/2 in. by 1/2 in. The dimensions of the counters and their distances from the target were chosen to maximize the ratio of the elastic p-p scatterings to the background.

Quasi-elastic scatterings of protons in the beam with protons in the nuclei of the nonhydrogen elements of the target were prime contributors to the background. Advantage was taken of the fact that these protons in the nuclei have an average Fermi momentum of 200 MeV/c. The orientation of this momentum is random, and its effect is to smear the trajectories of the scattering particles through an angle $\theta \approx [200(\text{MeV/c})]/[p_j(\text{MeV/c})]$ centered about the trajectories an elastic scattering would have had for the same center-of-mass-angle scattering. Here p_j represents the lab momentum of either scattered particle. This effect is largest for the counters that detect the slower proton of the scattering. The smaller and the farther back these counters are, the better the elastic scattering to background ratio becomes. However, a proton from an elastic scattering event at this angle has its trajectory smeared into an angle equal to twice the rms multiple-scattering angle θ_{rms} suffered by a particle as it emerged from the crystals. Once the angle in the plane of scattering subtended by a counter is equal to $2\theta_{rms}$, decreasing this angle more does not improve the "signal to noise" ratio, but merely decreases the counting rate. The lower array was positioned to detect the slower proton from a scattering event. The ratio of the width w_3 of one of its counters in the plane of the scattering to the distance from the target d_3 was chosen equal to $2\theta_{rms}$ for the average momentum of the proton detected in the array

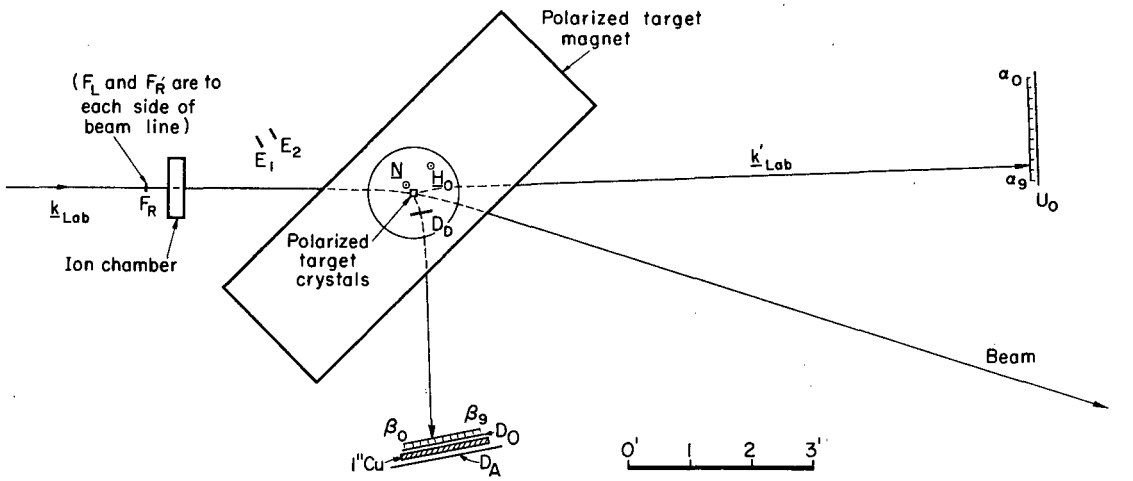

Fig. 8. Arrangement of the scintillation counters. The counter dimensions were:

a_i (2 × 1 × 1/2 in.) (ten counters)	U_0 (22 × 3/2 × 1.2 in.)
β_j (3/2 × 3/2 × 1/2 in.) (ten counters)	D_D (4-1/4 × 3/2 × 1/8 in.)
E_1, E_2 (2 × 1 × 1/2 in.)	D_0 (16 × 2 × 1/2 in.)
F_L, F_R (1/8 × 1/8 × 1/8 in.)	D_A (22 × 4-1/2 × 1/2 in.)

The direction of the normal to the scattering plane $\underline{N}$ and the direction of the external field $\underline{H}_0$ are indicated near the crystals. Since the proton has a positive magnetic moment, positive target polarization is parallel to $\underline{H}_0$.

$$\frac{w_3}{d_3} = 2\theta_{rms} = \frac{15}{p_3\beta_3}\sqrt{X_c}$$

where X_c = radiation length for the target, $X_c \approx 1/2$. Since the target is about 1-inch wide in the plane of the scattering, w_3 should be at least this large or larger. The spread of the quasi-elastic scatterings can further be taken advantage of by matching the angles that the lower and upper arrays subtend in the direction perpendicular to the plane of scattering. As an additional consideration, the total 10 counters in each array had to subtend an angular region in the plane of scattering large enough to be efficient, that is, to measure all accessible angles at one energy in two or three counter settings. The counters in each array were spaced as close to each other as the wrapppings would permit. This was done to minimize the effects from shifts in the beam's position or other changes that might cause elastic coincidences to shift in space. Since the counters were made adjacent, such a shift would merely result in the counts falling in the adjacent counter; and when one summed over several counters to obtain the hydrogen peak, one would still retain these counts. In this way the design and placement of the counters in the upper and lower array were determined.

Counters U_0 and D_0 were designed to cover the upper and lower arrays, respectively, and to be used in coincidence with the arrays to decrease accidental coincidences by requiring an extra coincidence. Counter D_D was designed to provide, along with the counters of the lower array and D_0, a spatial counter telescope that used only the crystals as a target. This avoided contributions to the background which would have come from events generated in the flanges of the vacuum system and the pole faces of the magnet.

Counter D_A was used with D_0 and D_D to provide another spatial telescope that had the crystals as a target. This coincidence was used as a monitor to normalize the length of reach run. The ion chamber and a two-counter spatial telescope, E_1E_2 (that used the ion

chamber as a target), were additional monitors independent of the normalizing monitor and the crystal target.

The center-of-mass scattering angles of events detected by the counter matrix were determined by kinematically tracing trajectories from the center of the target to the counter arrays in the laboratory frame. When the counter arrays were positioned to detect elastic scattering events, measurements in the laboratory system were taken to locate the arrays with reference to the polarized target. With this information, trial center-of-mass scattering angles were systematically chosen and the trajectories of the corresponding scattered particles were traced in the laboratory frame from the center of the target, through the magnetic field of the target magnet, and into the region of the upper array. Energy losses in the target were taken into account. When a trial trajectory intercepted the upper array, the trajectory of the conjugate particle of the scattering was traced out to determine into which lower counter it fell. Since these calculations were many and tedious, they were carried out on an IBM 7044 computer. When results were obtained, one could compare the location of the "hydrogen peaks" of the calculations to their locations in the experimental matrix. By varying parameters that described the location of the counter arrays and then noting any discrepancies in the positions of the calculated and experimental peaks, one could gain an estimate of the reliability of the angle determinations. In this manner we estimated that the calculated angles are correct to $\pm 1^\circ$ center of mass.

VII. ELECTRONICS

Figure 9(a) shows a schematic diagram of the electronics. The control system, called β-63 , was developed for this type of experiment by Frederick Kirsten and group. A master trigger was formed to "tell" the system when to process an event and store it. The master trigger was produced by a multiple coincidence of the following counters: $D_D - D_0 - \beta_i - U_0 - \alpha_j$, where i, j = 0 - 9. When a master trigger opened the circuit, the pulses from the upper and lower arrays that had generated standard pulses by means of discriminators were passed by a gate generated by the master pulse. Those signals on time with the gate, and thereby passed, set flip-flops for temporary storage. These flip-flops were interrogated to see whether one and only one signal existed in each array. If this were true, the event was considered valid, and one count was added to one of a hundred bins of a multichannel scaler (MCS). The address of the scaler was determined by the particular counters of the upper and lower arrays in which the coincidence occurred. The multichannel scaler was a RIDL pulse-height analyzer that had been modified to provide access to the address system. The address was set so that the counters in the upper array determined the ten's address and the counters in the lower array determined the unit's address. Thus the 10 by 10 matrix was stored in the one-hundred bins, 00 to 99.

To normalize the runs to the same number of incident protons, the monitoring circuits shown in Fig. 9(b) were used.

The $D_D - D_0 - D_A$ coincidences were counted and used to normalize the runs with different target polarizations.

The ion chamber and number of $E_1 - E_2$ coincidences were used to check on the functioning of the normalization monitor, and to determine whether any slight polarization dependence occurred in this monitor.

The singles rates in F_L and F_R were counted so that their ratio might tell when drifts occurred in the beam position.

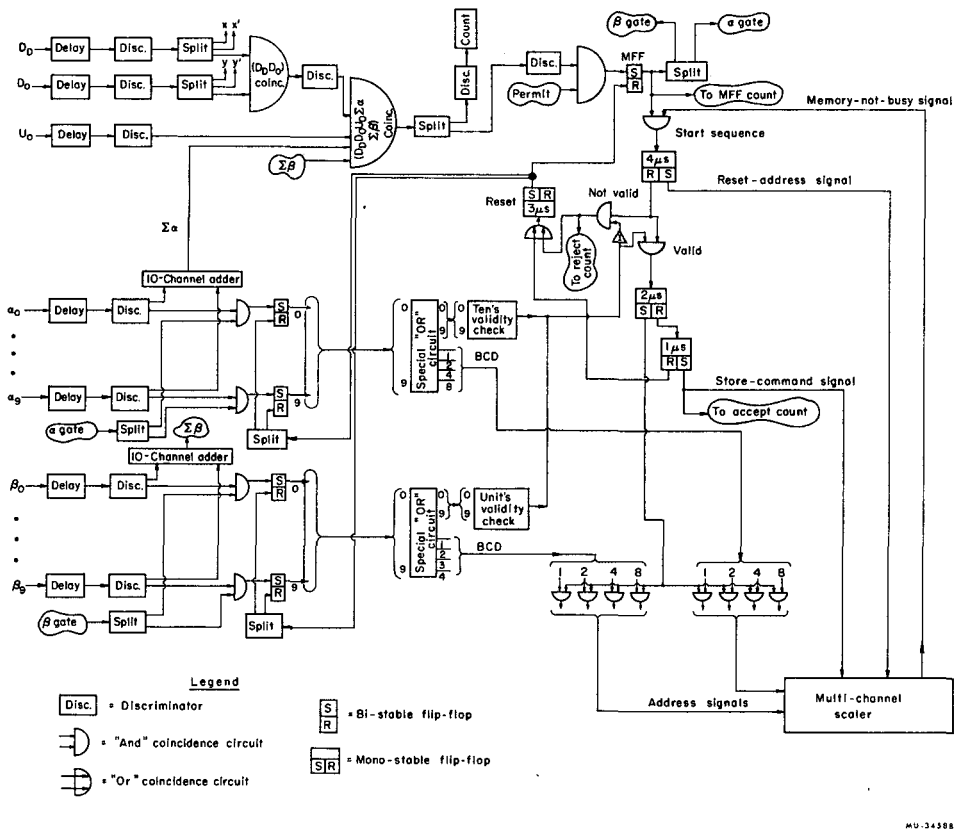

Fig. 9(a). Schematic of electronics used to process and store data.

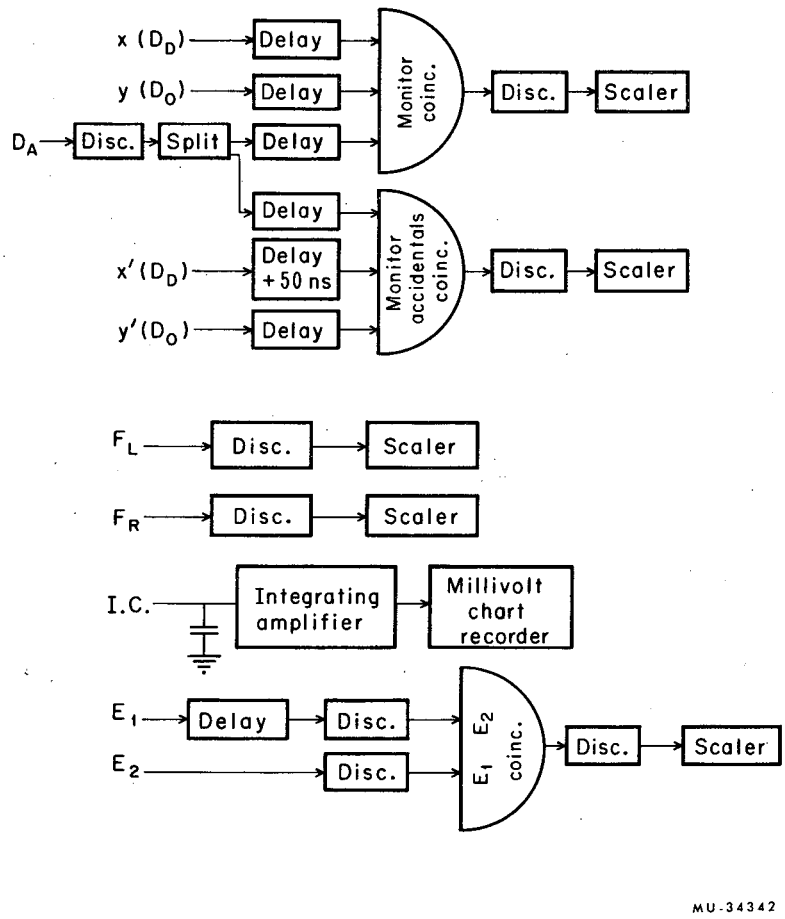

Fig. 9(b). Schematic of electronics used to provide monitoring information.

The length and smoothness of the beam spill was continuously observed by displaying the integrated singles rate of the U_0 counter on an oscilloscope. The oscilloscope was repetitively triggered at the same part of the acceleration cycle of the synchrocyclotron.

Most of the arithmetic operations in the analysis of data were handled by an electronic computer. At the site of the experiment the data were recorded by electric typewriter and simultaneously by paper punch on punched paper tape. These outputs included information for run identification as well as numerical data from all the scaling circuits. On an intermittent basis, data were also recorded from the NMR equipment used to measure the target polarization. Once each 12 hours of operation the punched paper tapes were transcribed onto magnetic tape for analysis by the computer.

VIII. ANALYSIS

In the center-of-mass system, a counter of the upper array defined a solid angle $\Delta\Omega$ at an angle θ. From Eq. (II-10), the number of counts in this counter that were accumulated during an ith run can be written as

$$N_i = m_i I_0 [1 + p_i P(\theta)] + m_i B \qquad \text{(VIII-1)}$$

where

m_i = monitor counts ($m_i \propto$ number of incident protons $\times$ solid angle of counter as long as the counter positions are held fixed.)

I_0 = unpolarized differential cross section for elastic p-p scattering in c.m. system

p_i = polarization of target

$P(\theta)$ = polarization parameter in p-p scattering

B = background contribution per unit monitor

$p_i = +|p_i|$ for positive target polarizations

and $\quad -|p_i|$ for negative target polarizations.

Positive target polarization means alignment of the proton spins predominantly parallel to the magnetic field and negative, antiparallel. Since the field at the polarized target bent the beam downward, one can see from Fig. 8 that the above statement is in agreement with the previous definition of p. In order to subtract the background, runs taken with the dummy target were normalized to the total of the runs taken with the polarized target by multiplying the matrix of the dummy target by the ratio R of the flat areas (see the example in Sec. X):

$$\sum_i^n N_i - R \sum_j^{n'} B_j = \sum_i^n m_i I_0 [1 + p_i P(\theta)] \qquad \text{(VIII-2)}$$

where B_j are the actual counts taken with the dummy target, $R = \frac{1}{2}\left[\left(\sum_C \sum_i N_i / \sum_C \sum_j B_j\right) + \left(\sum_D \sum_i N_i / \sum_D \sum_j B_j\right)\right]$, and C, D indicate summation over flat areas of the counter matrix. To

evaluate the polarization parameter $P(\theta)$ from the data, the hydrogen counts versus target polarization were fitted to a straight line by the method of least squares. This procedure is used because the target polarization varies from run to run. After background has been subtracted, the hydrogen counts G_i as a function of target polarization p_i can be written in the following form:

$$G_i \equiv N_i - m_i B = a + b\, p_i \qquad \text{(VIII-3)}$$

where

$a = I_0\, m_i$

$b = I_0\, m_i\, P(\theta)$

G_i = number of elastic p-p coincidences. (The background contribution $m_i B$ has been subtracted out.) (VIII-4)

For a least-squares fit one requires

$$\frac{\partial}{\partial a} \sum_i^n \left[G_i - (a + b\, p_i) \right]^2 = 0$$

$$\frac{\partial}{\partial b} \sum_i^n \left[G_i - (a + b\, p_i) \right]^2 = 0, \qquad \text{(VIII-5)}$$

which yields

$$\sum_i^n 2(G_i - a - b\, p_i) = 0$$

$$\sum_i^n 2(G_i - a - b\, p_i) p_i = 0.$$

Solving for a and b, one obtains

$$a = \frac{1}{n}\left(\sum_i^n G_i - b \sum_i^n p_i \right) = \frac{1}{n} \sum_i^n G_i - b\, \bar{p} \qquad \text{(VIII-6)}$$

where $\bar{p} = \dfrac{\sum_i^n p_i}{n}$

and

$$b = \frac{1}{n\left(\overline{p^2} - \bar{p}^2\right)} \sum_i^n G_i (p_i - \bar{p}) \,. \qquad \text{(VIII-7)}$$

We define $Q_i \equiv p_i - \bar{p}$ and rewrite a and b as

$$a = \frac{1}{n} \sum_i^n G_i - \frac{\bar{p}}{\langle Q^2 \rangle} \sum_i^n G_i Q_i \qquad \text{(VIII-8)}$$

$$b = \frac{1}{n \langle Q^2 \rangle} \sum_i^n G_i Q_i \qquad \text{(VIII-9)}$$

where

$$\langle Q^2 \rangle \equiv \frac{1}{n} \sum_i^n Q_i^{\,2} = \left(\overline{p^2} - \bar{p}^2\right).$$

Substitution of (VIII-8) and (VIII-9) into (VIII-4) gives

$$P(\theta) = \frac{\epsilon}{1 - \bar{p}\,\epsilon} \,, \qquad \text{(VIII-10)}$$

where

$$\epsilon \equiv \frac{\sum_i^n G_i Q_i}{\sum_i^n G_i \langle Q^2 \rangle} \,.$$

In this derivation the monitor counts m_i for each ith run have all been assumed to be equal. Since m_i is proportional to the number of incident protons, it is a measure of the length of the run. The runs may not always be of equal length, and in order to take this into account must make the least-squares fit to $(a+bp_i)$ of the elastic p-p coincidences

per unit monitor, G_i/m_i, and weight each term by the number of monitor counts m_i. Thus we perform a least-squares fit to the more general form:

$$\frac{\partial}{\partial a}\sum_i^n m_i\left[\frac{G_i}{m_i} - (a + b\,p_i)\right]^2 = 0$$

$$\frac{\partial}{\partial b}\sum_i^n m_i\left[\frac{G_i}{m_i} - (a + b\,p_i)\right]^2 = 0\,, \qquad \text{(VIII-11)}$$

which give

$$\sum_i^n G_i - a\sum_i^n m_i - b\sum_i^n m_i\,p_i = 0$$

$$\sum_i^n G_i\,p_i - a\sum_i^n m_i\,p_i - b\sum_i^n m_i\,p_i^2 = 0\,.$$

In a manner similar to the previous derivation, the simultaneous solution of these equations yields the following expression $P(\theta)$:

$$P(\theta) = b/a$$

$$P(\theta) = \frac{\epsilon}{1 - \bar{p}\,\epsilon}\,, \qquad \text{(VIII-12)}$$

where

$$\epsilon = \frac{\sum_i^n G_i\,Q_i}{\sum_i^n G_i\,\langle Q^2\rangle}$$

and here

$$\bar{p} \equiv \frac{\sum_i^n m_i\,p_i}{\sum_i^n m_i}\,, \qquad Q_i \equiv p_i - \bar{p}\,,$$

$$\langle Q^2\rangle \equiv \frac{\sum_i^n m_i\,Q_i^2}{\sum_i^n m_i} = \left(\frac{\sum_i^n m_i\,p_i}{\sum_i^n m_i}\right)^2 + \frac{\sum_i^n m_i\,p_i^2}{\sum_i^n m_i}\,.$$

One can see that the result of this more general form is to use m_i as a weighting factor in performing averages. Up to here we have neglected the background, but we next include its consideration. In order to take into account the background subtraction one notes that

$$\sum_i^n N_i Q_i = \sum_i^n m_i I_o [1 + p_i P(\theta)] Q_i + \sum_i^n B\, m_i Q_i \quad .$$

Since $$B \sum_i^n m_i Q_i = B \sum_i^n m_i \left(\frac{\sum_i^n m_i p_i}{\sum_i^n m_i} - \bar{p} \right) = 0 \quad ,$$

we have

$$\sum_i^n N_i Q_i = \sum_i^n G_i Q_i \quad . \qquad \text{(VIII-13)}$$

Also Eq. (VIII-2) is, by definition,

$$\sum_i^n N_i - R \sum_j^{n'} B_j = \sum_i^n G_i \quad . \qquad \text{(VIII-14)}$$

Combining Eqs. (VIII-13) and (VIII-14) with (VIII-10) one obtains the final form for computing $P(\theta)$:

$$\epsilon = \frac{\sum_i^n N_i Q_i}{\left(\sum_i^n N_i - R \sum_j^{n'} B_j \right) \langle Q^2 \rangle}$$

$$P(\theta) = \frac{\epsilon}{1 - \bar{p}\epsilon} \quad . \qquad \text{(VIII-15)}$$

When making an experimental measurement of $P(\theta)$, we attempted to keep all factors constant except the target polarization, which was reversed approximately every 40 minutes. Magnet currents and helium-bag pressure were usually checked every 3 hours and counter voltages every 4 hours. The beam spill was continuously observed by the

operator. For each run, F_L divided by F_R, monitor coincidences divided by ion chamber volts, and the length of the run in minutes were graphed that changes might be observed in any of the conditions. The beam intensity was chosen so that changes in beam intensity, up or down, by a factor of two made no discernible difference in the ratio of the hydrogen peak to the background. The NMR differential signal of the polarized target was continuously recorded on a chart, and digitized examples were read out before each reversal of the target polarization. Every 12 hours, the microwaves to the target were turned off and the crystals were allowed to come to thermal equilibrium with the helium bath. Three NMR signals were recorded under these conditions, and the vapor pressure of the helium was read for each signal.

In analyzing the runs that were taken for each setting of the counter positions, we made graphs for each upper counter. The number of counts in each successive run was plotted for each lower counter to determine the consistency of the measurements. The monitor coincidences were checked for any polarization dependence of the monitor circuit by plotting these counts versus ion chamber volts and versus (E_1E_2) coincidences for each run. At three counter positions where the asymmetry in scattering was large and the slower scattered proton had sufficient energy to penetrate 1-in. slab of copper between counters D_0 and D_A, an average polarization dependence of 1% was found between the runs for positive target polarization and negative target polarization. More counts appeared in monitor coincidence for positive target runs than for negative runs for equal amounts of charge accumulated by the ion chamber. For a set of runs with negative polarization, the magnitudes of the negative target polarizations were roughly equal. The same was true for the magnitudes of the positive polarizations. Thus a first-order correction for polarization dependence of the monitor was made by multiplying the number of counts in the monitor scaler for each negative run by a factor equal to the ratio of the average positive divided by average negative monitors. At the majority of counter positions no such correction was needed.

IX. ERRORS

For convenience we write Eq. (VIII-13) again:

$$\epsilon = \frac{\sum_i^n N_i Q_i}{\left(\sum_i^n N_i - R \sum_j^{n'} B_j\right) \langle Q^2 \rangle}$$

$$P(\theta) = \frac{\epsilon}{1 - \bar{p}\epsilon} \quad .$$

The runs were taken with the magnitude of the positive polarizations of the target roughly equal to the magnitude of the negative polarizations. Thus in practice $\bar{p}$ was always small, and in fact $\bar{p} < 0.1$ for all counter positions. In practice ϵ was always less than 0.5. With the assumption that the error on $\bar{p}$ is always negligible, the error analysis is simplified. We compute the errors in ϵ and set $\Delta P = (\partial P/\partial \epsilon)\Delta\epsilon$, where $\partial P/\partial \epsilon = 1/(1 - \bar{p}\,\epsilon)^2$. The square of the error in ϵ, $\Delta\epsilon^2$, is computed by combining the quadrature, the errors in the independent measurements times their weights:

$$\Delta\epsilon^2 = \left[\sum_i^n \left(\frac{\partial \epsilon}{\partial N_i} \Delta N_i \right)^2 + \left(\frac{\partial \epsilon}{\partial R} \Delta R \right)^2 + \left(\frac{\partial \epsilon}{\partial \Sigma B_j} \Delta \Sigma B_j \right)^2 + \sum_i^n \left(\frac{\partial \epsilon}{\partial m_i} \Delta m_i \right)^2 + \sum_i^n \left(\frac{\partial \epsilon}{\partial p_i} \Delta p_i \right)^2 \right]$$

(IX-1)

(a) The first source of error $(\partial \epsilon/\partial N_i)\Delta N_i$ is determined by the statistics of the counts in the hydrogen-peak region for each a counter; $\Delta N_i = \sqrt{N_i}$.

(b) The second source of error, $(\partial\epsilon/\partial \Sigma B_j)\Delta \Sigma B_j$, is determined by the statistics of the counts of the dummy target in the region where the hydrogen peaks would have been; $\Delta \Sigma B_j = \sqrt{\Sigma B_j}$.

(c) The third source, $(\partial \epsilon / \partial R)\Delta R$, is determined from the statistics in the flat regions of the matrix that are used to normalize the dummy target;

$$\Delta R = \frac{1}{2}\left[\left(\frac{\sum_C \sum_i N_i}{\sum_C \sum_j B_j}\right)^2\left(\frac{1}{\sum_C \sum_i N_i} + \frac{1}{\sum_C \sum_j B_j}\right) + \left(\frac{\sum_D \sum_i N_i}{\sum_D \sum_j B_j}\right)^2\left(\frac{1}{\sum_D \sum_i N_i} + \frac{1}{\sum_D \sum_j B_j}\right)\right]^{\frac{1}{2}}$$

where C and D indicate summation over the flat areas of the matrix.

(d) The fourth source $(\partial \epsilon / \partial m_i)\Delta m_i$ is determined from the statistics in the monitor coincidences used to normalize the runs; $\Delta m_i = \sqrt{m_i}$.

(e) The fifth source $(\partial \epsilon / \partial p_i)\Delta p_i$ arises from the estimation of the average polarization of the target during a run. The error in p_i, Δp_i, is determined from the scatter in a plot of calculated polarizations versus peak-to-peak recorded signals of the NMR proton resonance of the target; Δp_i ranged from 4.5% to 5.5%.

(f) In addition to the above sources of error an additional systematic error arose from measurements of (a) the area of the TE proton resonance signal and (b) the temperature of the liquid helium bath when the signal was recorded. The accuracy with which the oil manometer indicated the vapor pressure of the liquid helium contributed an uncertainty of 3% in the value of the absolute polarization of the average TE signal. The average area of the TE was estimated to be good to ±5%. Combining these errors in quadrature gave a systematic error of 5.83% to be added, in quadrature, to the other sources of error.

If the polarization is not uniform in the target, a systematic error can be introduced. Early in the experiment, after some data had been taken, a small beam of approximately 1/4 in. diameter was focused on various parts of the target and the asymmetry in counting rate for each part was measured. In this manner a contour diagram of polarization in the target was obtained. It was found that scattering

from the top, side, and bottom edges produced an asymmetry almost twice that produced from the center. A spot halfway between the side edge and center produced an intermediate asymmetry. Figure 10 shows results of the probing. Nonuniform target polarization could arise from several sources: a nonuniform magnetic field across the volume of the crystals, nonpenetration of the microwaves into the crystals, a temperature distribution within the crystals, and nonuniform radiation damage to the crystals. The magnetic field had been measured to provide a uniform field over the volume of the crystals, so this source of nonuniformity was thought to be negligible. In practice, the other effects were difficult to separate reliably, and any of them may have been important.

After the target was probed, the crystals were taken apart. It was realized that the detection coils described in Sec. V had been placed too close to the crystals. At some points the edges of the crystals almost touched the coils. Thus the target polarization previously measured was not a true volume average but was very heavily weighted by the polarization at the edges of the crystal. A new cavity was fabricated in which the coils were spaced farther apart. No part of the crystals came within 1/4 in. of the coils. A new septum design was also made to increase the uniformity of the rf magnetic field within the coils. The old crystals had been greased with Kel-F fluorinated grease to protect the crystals from moisture. The grease, however, stuck the crystals together and prevented liquid helium from covering each individual crystal. The new crystals were left ungreased to minimize any temperature gradients, and every point in the target was then within 1/8 in. or less of the liquid helium bath.

Before the target was probed, the size of the beam spot was equal to the size of the crystals. Afterwards, the beam spots were made 1.5 to 2 times the size of the target to avoid nonuniformity of polarization by radiation damage and to ensure that the beam sampled the target uniformly.

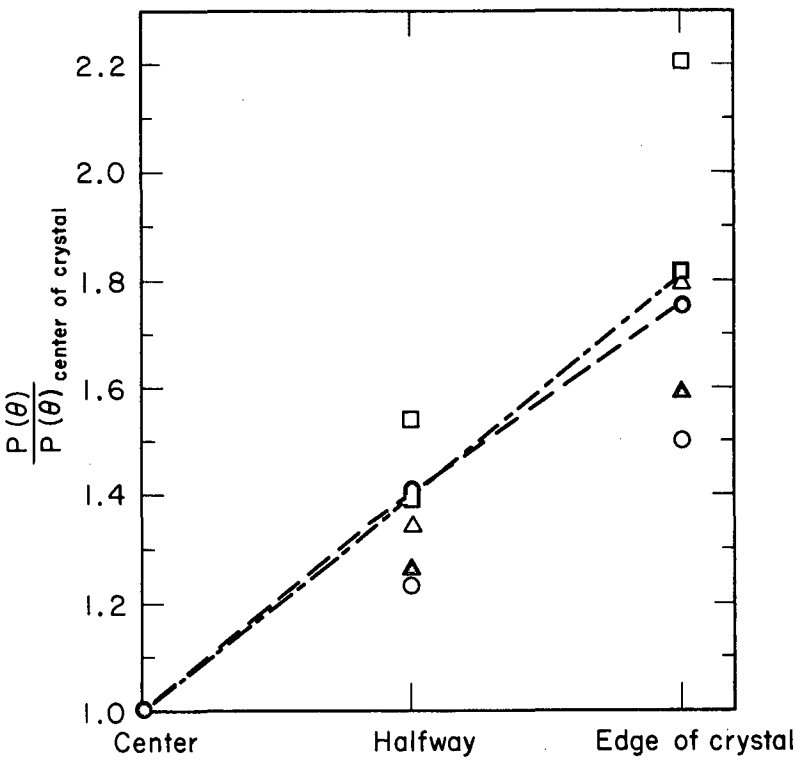

Fig. 10. The ratios of the polarization parameter measured with a small beam spot at the center of the crystal to that measured with the spot at the edge of the crystal and at a point half-way in between are plotted with solid circles. The small beam measurements at the top, side, and bottom edges gave identical results. As computed by the correction program, the same ratios for various choices of $T(x,y,z)$ are also shown. ●, experimental measurements; ○, $T \propto 1 + 10r$; ▲, $T \propto 1 + 2r + 2r^2$; △, $T \propto 1 + 4r^2$; , $T \propto \exp(r^2/R^2)$; □, $T \propto r^2$.

In summarizing the analysis of possible errors due to a non-uniform spatial distribution of polarization within the target crystals, one notes that there are two ways of avoiding any error. First, if the target is uniformly polarized there is no difficulty. Second, if the rf system samples the target polarization uniformly over the target volume and the beam uniformly irradiates the target, then there is no error. Since it is difficult to guarantee uniform target polarization, we have generally adopted the second approach to getting the right answers.

The data measured at energies of 736, 679, and 328 MeV were taken under the new conditions after the target probing. The data measured at the energy of 614 MeV were taken previous to the probing.

To estimate the magnitude of the systematic error introduced by the above effects, we calculated the ratio of the measured target polarization M_T to the effective target polarization E_T:

$$M_T = \frac{\iiint T(x,y,z)\, S(x,y,z)\, dx\, dy\, dz}{\iiint S(x,y,z)\, dx\, dy\, dz}$$

$$E_T = \frac{\iiint T(x,y,z)\, B(x,y)\, dx\, dy\, dz}{\iiint B(x,y)\, dx\, dy\, dz}\,, \qquad \text{(IX-2)}$$

where $B(x,y)$ represents the distribution of the beam intensity incident upon the target, $S(x,y,z)$ represents the sensitivity of the detection coils to points within its volume, and $T(x,y,z)$ represents the target polarization as a function of position within the target. The coordinates x, y, z comprise an orthogonal coordinate system with z in the direction of the incident beam. To correct for this source of error, the measured $P(\theta)$ is multiplied by this factor:

$$P(\theta)_{\text{corrected}} = \frac{M_T}{E_T}\, P(\theta)_{\text{measured}}\,. \qquad \text{(IX-3)}$$

The beam distribution was approximated by a gaussian

$$B(x,y) = \exp\left(\frac{(x-x_0)^2 + (y-y_0)^2}{2\sigma^2}\right). \qquad \text{(IX-4)}$$

where σ is standard deviation.

The sensing function $S(x, y, z)$ was approximated empirically by reproducing a scale model of the coils and cavity configuration with conducting paint on resistive carbon paper. The rf magnetic-field configuration of the coils was taken from the electrical equipotential lines traced on the paper. The sensing function was taken proportional to the energy density of the rf magnetic field. The field was taken as proportional to the density of the equipotential lines. An analytic fit to the line density was made:

$$H_{rf} \propto (1+y^2)\left[1 + 64\, y^8 \left(z - \tfrac{1}{2}\right)^4\right](1 + 10\, y^8 x^4) \quad , \qquad \text{(IX-5)}$$

and the sensing function S was:

$$S(x, y, z) = (H_{rf})^2 \, . \qquad \text{(IX-6)}$$

The ratio $\left(\frac{H_{rf\ max}}{H_{rf\ min}}\right)^2$ for various parts of the crystals is given in Fig. 11. After $T(x, y, z)$ was chosen, the factor 64 was changed to 80 and produced a 3% change in M_T/E_T. The factor 10 was changed to 40 and produced 1/2% change. The factor 1 in front of y^2 was changed to 2 and produced a 5% change.

The polarization density $T(x, y, z)$ was chosen by trial and error to give a best fit to the results of target probing shown in Fig. 10, which also shows the fit made by various distributions.

$$T(x, y, z) \propto \exp\left(r^2/R^2\right) \qquad \text{(IX-7)}$$

(where $r^2 = x^2 + y^2 + z^2$ and R = radius of the crystal) provided a reasonably good fit. Pictures of the beam spots used in the different energies are shown in Fig. 12 along with the relationship of the crystals to the detecting coils.

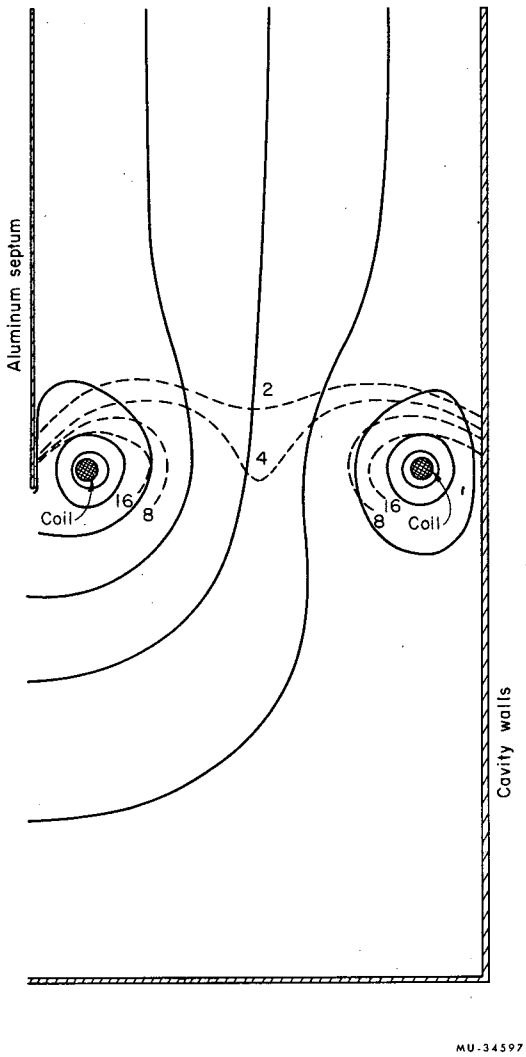

Fig. 11. This figure shows a sketch of a bottom-quarter section of the NMR coil configuration with the viewer looking parallel to the aluminum septum (perpendicular to the direction of the incident proton beam). The rf magnetic-field lines are represented by the solid lines. The dotted lines depict contours of constant $(H_{rf\,max}/H_{rf\,min})^2$ in the region occupied by the crystals. The normalization is such that the quantity has a value of 1 in the center of the crystals.

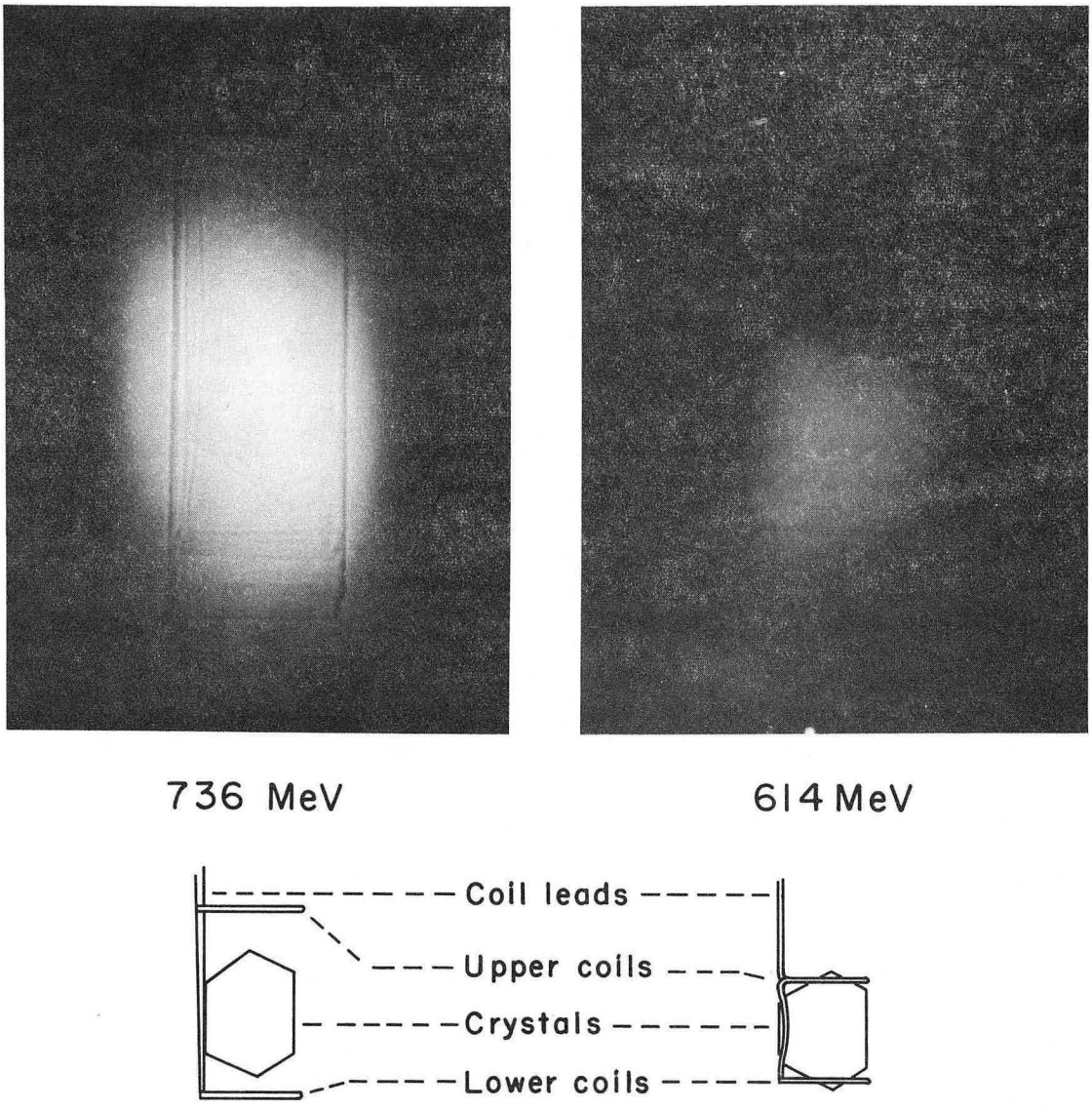

Fig. 12. The picture in the upper-left-hand corner shows the beam spot used at 736 MeV; the geometry of the coils and crystals is sketched immediately below. The picture in the upper-right-hand corner shows the beam spot at 614 MeV with a similar sketch below. At the energies of 328 and 679 MeV, the beam-spot sizes were similar to that at 736 MeV and the coil-crystal geometry was identical.

The correction factor M_T/E_T for the energy of 614 MeV is 1.24. The $P(\theta)$ for this energy have been corrected by this factor with a systematic error of ±12%. For the three energies 736, 679, and 328 MeV the coils had been moved back and the uniform cooling of crystals improved. No probing of the target was done after these changes. Using the polarization distribution of Eq. (IX-6) and the coil crystal geometry indicated in Fig. 12 one can place an upper limit of 1.06 on this correction. Since the temperature distribution in the target was made more uniform, any correction to this set of data should be significantly less than this maximum limit. The data on $P(\theta)$ presented for these energies have not been corrected for this effect, but a systematic error of $\binom{+3}{-0}$ % has been assigned.

X. SAMPLE CALCULATION

We show a sample calculation of $P(\theta)$ using an upper array counter a_8, which corresponded to a center-of-mass angle of $68.5° \pm 1°$ at a lab kinetic energy of 736 MeV. The runs in Table III were taken at this counter position. Each run was gated off by the ion chamber at approximately 10 volts with an 1.08-μF capacitor. The length of an average run was 13 minutes. Two successive runs with the same sign of target polarization were taken, and the direction of the target polarization was then reversed. The average beam intensity was 3.8×10^8 protons/second, with a duty factor of two assumed for the cyclotron. Figures 13, 14, 15 are graphs of monitors divided by ion chamber, F_L divided by F_R, and the length of the run in minutes--plotted respectively for each polarized run.

The F_L/F_R counters ratio indicates a steady beam shift from run 12 to run 19. Equal numbers of positive and negative runs exist in this set. The magnet currents were checked at this point, and any drift is considerably less for runs 21 to 28. No polarization dependence of the monitor is discernible in the plot of monitor divided by ion chamber.

Figure 16 shows the coincidences for each run of the upper counter with each successive lower counter. The coincidences taken with positive (o) and negative (**o**) target polarization are displayed in temporal sequence.

The full 10 by 10 matrix is reproduced in Table IV for run 12 as an example. Table III contains the row of the matrix that corresponded for each run to counter a_8. Tables V and VI are, respectively, the matrix formed by summing the runs with the polarized target and the matrix formed by summing the runs with the dummy target. The areas, indicated as C and D, were used for normalization of the dummy target data.

Table III. List of runs taken at 736 MeV and center-of-mass angle $\theta_{c.m.} = 68.5$ deg. The coincidence between the upper counter at this angle (α_8) and each β counter are also given for each run.

Run	Target polarization	β_0	β_1	β_2	β_3	β_4	β_5	β_6	β_7	β_8	β_9
12	-	86	152	486	958	505	210	165	175	173	163
13	-	80	151	460	953	491	196	190	185	182	181
14	+	77	184	608	1229	613	197	144	160	184	162
15	+	74	164	580	1260	569	194	179	169	134	177
16	-	72	155	460	960	477	184	176	176	155	149
17	-	74	165	476	924	513	192	186	179	161	166
18	+	84	164	652	1199	561	206	183	166	174	156
19	+	66	154	557	1175	583	190	144	146	153	165
21	-	81	152	478	951	481	194	175	188	184	178
22	-	83	149	467	992	503	210	177	190	160	171
23	+	77	179	631	1352	634	176	168	170	179	170
24	+	75	171	552	1303	639	218	160	181	173	132
25	-	65	144	470	1010	482	201	168	182	166	181
26	-	90	162	448	1037	512	169	174	176	146	194
27	+	75	170	614	1234	574	188	173	185	179	170
28	+	78	167	602	1275	576	183	171	206	145	162
42	Dummy target	79	107	161	152	162	170	146	170	150	118
44	Dummy target	88	118	183	176	193	177	165	156	129	152
45	Dummy target	88	140	133	175	174	189	167	166	148	127
46	Dummy target	83	122	160	201	171	177	183	160	163	132

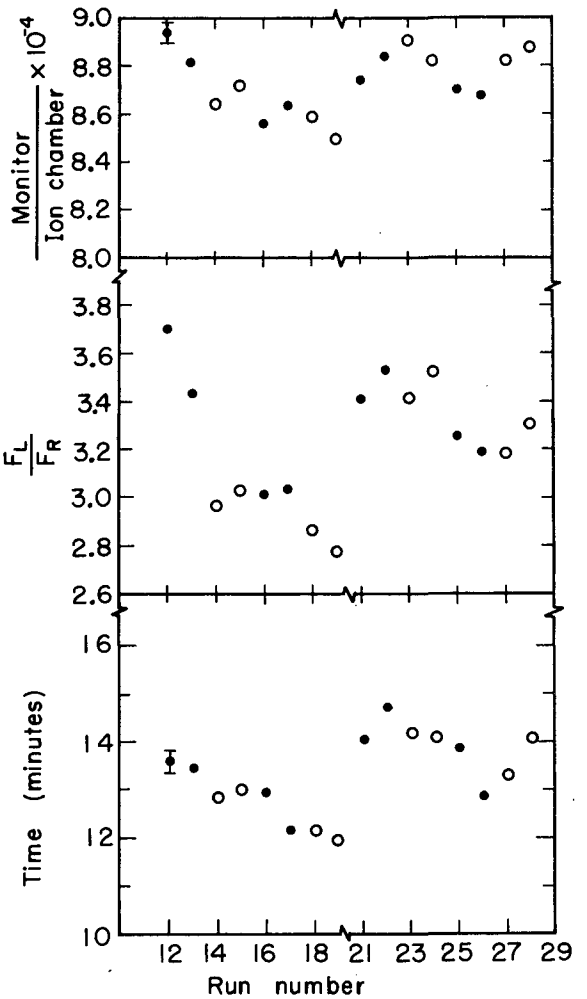

Fig. 13. Monitor counts/ion chamber versus run number for runs taken at 736 MeV, $\theta_{c.m.} = 68.5°$.

Fig. 14. F_L/F_R versus run number (736 MeV, $\theta_{c.m.} = 68.5°$).

Fig. 15. Length of run in minutes versus run number (736 MeV, $\theta_{c.m.} = 68.5°$).

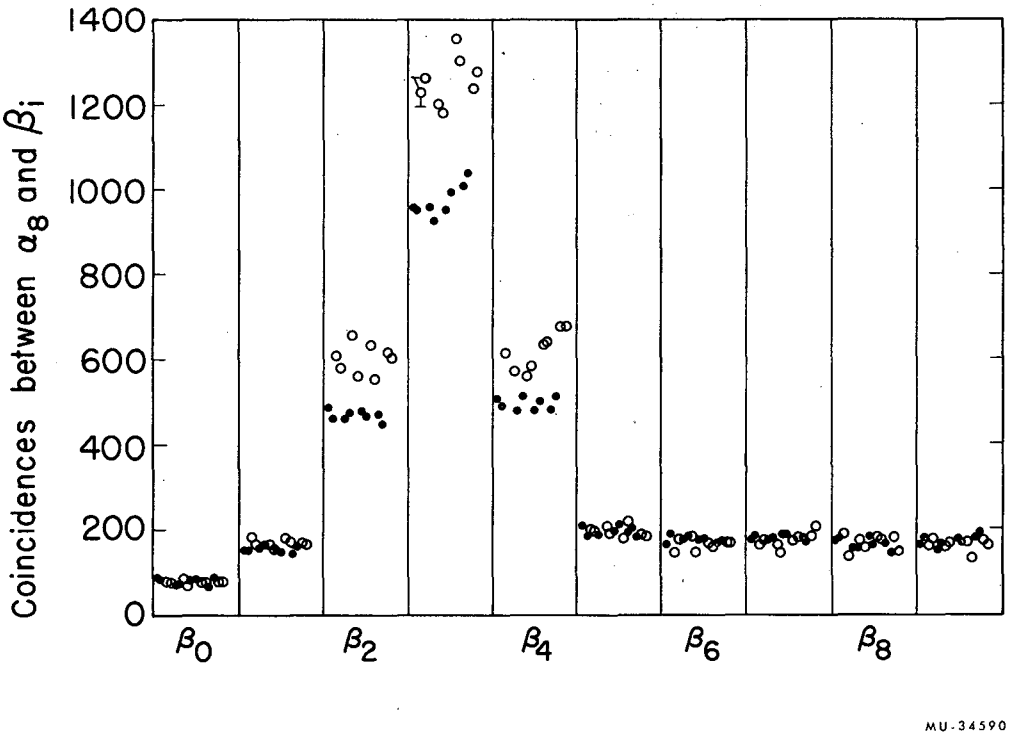

Fig. 16. Coincidences between counter α_8 and each β counter plotted in temporal sequence.

Table IV. Ten-by-ten matrix of counter coincidences stored during Run 12. Each row corresponds to an alpha counter. Each column corresponds to a beta counter.

4	4	12	25	21	23	23	22	31	41
12	13	22	21	34	34	32	60	59	147
20	16	29	52	34	49	65	69	180	335
26	41	53	51	65	80	108	186	523	457
37	62	82	94	99	134	290	882	576	220
50	65	78	115	121	321	851	530	204	162
51	83	101	169	350	898	575	198	186	165
56	76	167	435	984	576	193	165	173	174
86	152	486	958	505	210	165	175	173	163
137	544	930	463	177	152	158	179	177	169

Table V. Coincidence matrix of the total counts accumulated during all the runs taken with the polarized target at 736 MeV, $\theta_{c.m.}$ = 68.5 deg.

105	159	215	258	276	349	343	385	458	799
188	262	342	396	503	576	595	734	861	2265
246	393	569	658	689	815	921	1273	2859	5577
401	602	780	901	1040	1182	1439	3021	8416	6884
583	881	1222	1524	1697	2129	4757	14853	9754	3425
743	1068	1384	1719	2025	5541	15041	9844	2891	2610
849	1227	1626	2280	6031	16246	9505	3044	2630	2770
		Area C							
979	1519	2382	7244	16380	9729	3047	2897	2663	2750
1237	2583	8541	17812	8713	3108	2733	2834	2648	2677
2516	9723	17251	8320	2930	2833	2723	2795	2722	2598
								Area D	

The data taken with the dummy target are normalized with the outlined areas, C and D.

Table VI. Coincidence matrix of the total counts accumulated during all the runs taken with the dummy target at 736 MeV, $\theta_{c.m.}$ = 68.5 deg.

40	37	49	60	63	78	85	65	83	62
52	80	111	107	121	128	117	155	140	122
72	108	131	149	194	199	216	210	213	220
109	147	220	251	282	250	275	318	344	353
192	240	334	354	366	485	473	566	531	484
232	296	389	482	480	578	620	620	498	490
266	351	444	516	570	679	612	570	524	498
	Area C								
328	386	508	613	705	700	652	577	503	531
338	487	637	704	700	713	661	652	590	529
374	641	775	762	665	693	674	616	583	541
							Area D		

$$R = \frac{1}{2}\left(\frac{\sum_c \sum_i N_i}{\sum_c \sum_\gamma B_\gamma} + \frac{\sum_D \sum_i N_i}{\sum_D \sum_\gamma B_\gamma}\right) = \frac{1}{2}\left(\frac{15106}{4156} + \frac{33028}{6714}\right)$$

$$R = 4.277$$

The sum matrix of the dummy target data is then multiplied by the ratio R. Figure 17 shows the results of the dummy background normalization. It displays the sum of the polarized target runs and the normalized dummy target runs for counter α_8. The hydrogen peak for α_8 occurs in the lower counters $\beta_2\beta_3\beta_4$. The counts in these three bins are summed to provide the counts in the hydrogen peak and also to provide the background counts for subtraction. Table VII lists the quantities needed to compute $P(\theta)$.

$$\epsilon = \frac{\sum_i^n N_i Q_i}{\left(\sum_i^n N_i - R\sum_\gamma^n B_\gamma\right)\langle Q^2\rangle}$$

$$\epsilon = 0.365$$

$$P(\theta) = \frac{\epsilon}{1 - \bar{p}\,\epsilon}$$

$$P(\theta) = 0.364$$

The error ΔP in P is computed as follows:

$$\Delta P = \frac{\partial P}{\partial \epsilon}\left\{\sum_i^n \left(\frac{\partial \epsilon}{\partial N_i}\Delta N_i\right)^2 + \left(\frac{\partial \epsilon}{\partial R}\Delta R\right)^2 + \left(\frac{\partial \epsilon}{\partial \Sigma B_j}\Delta \Sigma B_j\right)^2 + \sum_i^n \left(\frac{\partial \epsilon}{\partial m_i}\Delta m_i\right)^2 + \sum_i^n \left(\frac{\partial \epsilon}{\partial p_i}\Delta p_i\right)^2\right\}^{1/2}$$

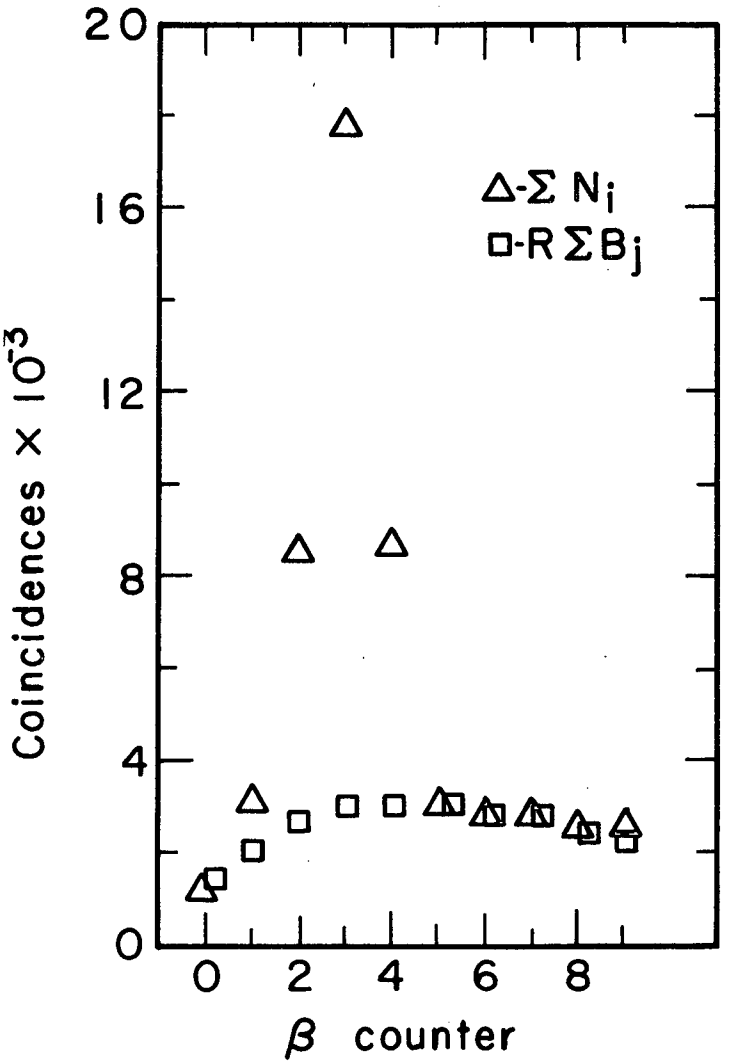

Fig. 17. Plot of the sum of the coincidences between counter a_8 and each β counter taken with the crystal target and with the dummy target. The coincidences taken with the dummy target have been normalized as indicated in the text.

Table VII. Data used for the sample calculation of $P(\theta)$.

Run no.	N_i	p_i	m_i	$m_i p_i$	p_i^2	$m_i p_i^2$	Q_i	$N_i Q_i$	$N_i Q_i$
12	1949	-0.425	1889927	-803219	0.180625	3141368	-0.4153	336	-809
13	1904	-0.415	1875346	-778269	0.172225	322981	-0.4053	313	-772
14	2450	+0.425	1857976	+789640	0.180625	335597	+0.4347	463	+1065
15	2409	+0.449	1864089	+836976	0.201601	375802	+0.4587	507	+1105
16	1897	-0.430	1848645	-794917	0.184900	341814	-0.4203	335	-797
17	1913	-0.425	1854500	-788163	0.180625	334969	-0.4157	330	-794
18	2412	+0.401	1849678	+741721	0.160801	297430	+0.4107	407	+991
19	2315	+0.425	1840528	+782224	0.180625	332445	+0.4347	437	+1006
21	1910	-0.478	1864676	-891315	0.228484	426049	-0.4683	419	-894
22	1962	-0.459	1874271	-860290	0.210681	394873	-0.4493	396	-882
23	2617	+0.391	1885130	+737086	0.152881	288201	+0.4007	420	+1049
24	2494	+0.391	1876609	+733754	0.152881	286898	+0.4007	400	+999
25	1962	-0.391	1869823	-731101	0.152881	285860	-0.3813	285	-748
26	1997	-0.430	1864237	-801622	0.184900	344697	-0.4203	353	-839
27	2422	+0.401	1882319	+754810	0.160801	302679	+0.4107	409	+995
28	2453	+0.415	1883127	+781498	0.172225	324322	+0.4247	443	+1042
		$\Sigma\lvert p_i\rvert$=6.751		Σ-6448896 Σ+6157709			Σ+3.3756 Σ-3.3754		Σ+8252 Σ-6535
Σ	35066		29880881	-291187		5335985	+0.0002	6253	+1717
$\Sigma/16$	2192	0.422	1868680						

ΣB_j = 2041 R = 4.277

$R\Sigma B_j$ = 8729

$(\Sigma N_i - R\Sigma B_j)$ = 26337

$$\overline{p} = \frac{\Sigma m_i p_i}{\Sigma m_i} = \frac{-291187}{29880881} = -0.0097$$

$$\overline{p^2} = \frac{\Sigma m_i p_i^2}{\Sigma m_i} = \frac{5335985}{29880881} = 0.178575$$

$$\langle Q^2 \rangle = \overline{p^2} - (\overline{p})^2 = 0.1785$$

$$\sqrt{\langle Q^2 \rangle} = 0.4225$$

$$\frac{\partial P}{\partial \epsilon}\sqrt{\sum_i^n\left(\frac{\partial \epsilon}{\partial N_i}\Delta N_i\right)^2} = \frac{1}{(1-\bar{p}\epsilon^2)}\,\frac{1}{\langle Q^2\rangle(\Sigma N_i - R\Sigma B_j)}\left\{\Sigma N_i Q_i^2 + [\Sigma N_i - 2(\Sigma N_i - R\Sigma B_j)]\left(\frac{\Sigma N_i Q_i}{\Sigma N_i - R\Sigma B_j}\right)^2\right\}^{1/2}$$

$$= 0.0170 \quad .$$

$$\frac{\partial P}{\partial \epsilon}\,\frac{\partial \epsilon}{\partial R}\Delta R = \frac{1}{(-\bar{p}\epsilon)^2}\,\frac{\epsilon\Sigma B_j}{(\Sigma N_i - R\Sigma B_j)}\Delta R$$

$$\Delta R = \frac{1}{2}\left\{\left(\frac{\sum_c\sum_i N_i}{\sum_c\sum_j B_j}\right)^2\left(\frac{1}{\sum_c\sum_i N_i} + \frac{1}{\sum_c\sum_j B_j}\right) + \left(\frac{\sum_b\sum_i N_i}{\sum_b\sum_j B_j}\right)^2\left(\frac{1}{\sum_c\sum_i N_i} + \frac{1}{\sum_b\sum_j B_j}\right)\right\}^{1/2}$$

$$\Delta R = 0.046$$

$$\frac{\partial P}{\partial \epsilon}\,\frac{\partial \epsilon}{\partial R}\Delta R = 0.0013 \quad .$$

$$\frac{\partial P}{\partial \epsilon}\,\frac{\partial \epsilon}{\partial \Sigma B_j}\Delta\Sigma B_j = \frac{1}{(1-\bar{p}\epsilon)^2}\,\frac{R\epsilon}{(\Sigma N_i - R\Sigma B_j)}\sqrt{\Sigma B_j}$$

$$= 0.0027 \quad .$$

$$\frac{\partial P}{\partial \epsilon}\sqrt{\sum_i^n\left(\frac{\partial \epsilon}{\partial m_i}\Delta m_i\right)^2} = \frac{1}{(1-\bar{p}\epsilon)^2}\left\{\sum_i^n\left[\frac{\sqrt{m_i}}{(\Sigma N_i - R\Sigma B_j\langle Q^2\rangle\Sigma m_i}\left(\Sigma N_i Q_i\left[1-\frac{Q_i}{\langle Q^2\rangle}\right] - Q_i\Sigma N_i\right)\right]^2\right\}^{1/2}$$

$$\approx 0.00057 \quad .$$

$$\frac{\partial P}{\partial \epsilon}\sqrt{\sum_i^n\left(\frac{\partial \epsilon}{\partial p_i}\Delta p_i\right)^2} = \frac{1}{(1-\bar{p}\epsilon)^2}\,\frac{1}{(\Sigma N_i - R\Sigma B_j)\Sigma m_i\langle Q^2\rangle}\left\{\sum_i^n\left[\Delta p_i \times\left\{N_i\Sigma m_i - m_i\Sigma N_i - 2(\Sigma N_i - R\Sigma B_j)\epsilon m_i Q_i\right\}\right]^2\right\}^{1/2}$$

$$\approx 0.008 \quad .$$

$\Delta P \approx (0.017)^2 + (0.0013)^2 + (0.0027)^2 + (0.00057)^2 + (0.008)^2$

$\Delta P \approx 0.019.$

To this percentage error $(\Delta P/P = 5.2\%)$, a systematic error of 5.8% (from the area and polarization of the TE signal) is added in quadrature:

$$P = 0.364 \pm 0.028.$$

(The error from nonuniform polarization in the target has not been included).

XI. RESULTS

The measured values of the polarization parameter $P(\theta)$ in elastic proton-proton scattering are presented in the Tables VIII through XI and graphed in the Figs. 18 through 22. Given with each of the values of the polarization parameter is the corresponding center-of-mass angle $\theta_{c.m.}$ and the negative of the invariant square of the four-momentum transfer t. For elastic p-p scattering, t is related to $\theta_{c.m.}$ by the expression $t = -2k^2(1-\cos\theta_{c.m.})$, where k^2 is the square of the incident three-momentum in the center-of-mass system.

At the energy of 614 MeV, measurements were made to an angle as small as $\theta_{c.m.} = 40°$. The measurements at these smaller angles, however, were discarded because the spatial locations of the p-p interactions in the target crystals came, at these angles, predominantly from the edges of the crystal. This was due to the fact that at smaller angles the recoil proton emerged with less energy and suffered increased energy losses. When the energy of the recoil proton corresponded to a range barely sufficient to emerge from the crystals, the location of the interactions in the crystal target became important; and only those interactions near the edges of the crystals were observed. The correction factor, which we computed to correct the measurements for nonuniformity of polarization in the target, assumed that the only spatial distribution of interactions in the target arose from the Gaussian distribution of the beam particles. This correction factor could then be applied only at angles where the range of the recoil particle was not small enough to begin influencing the spatial locations of the interactions.

The angle at which the range of the recoil particle did begin to influence these locations was easily determined by noting the angle at which the counting rate began to fall off rapidly; and measurements at angles smaller than this were discarded. In principle, of course, one could compute a correction factor for measurements of these smaller angles, but such a computation would require that we more accurately

know the distribution of the polarization within the target. The values of the polarization parameter $P(\theta)$ given in Table IX and plotted in Fig. 19 have been corrected by the factor of 1.24 discussed in Sec. IX.

At the energies of 328, 679, and 736 MeV, the same considerations occur. However, as we have previously described, before we made the measurements at these energies, we had attempted to increase the uniformity of polarization within the target. To accomplish this, we had increased the area of contact of the individual crystals with liquid helium bath and avoided nonuniform radiation damage to the crystals. Evidence that some success was attained can be found by considering the values of the polarization parameter at the corresponding small angles. At these angles (42.0 to 32.5° for 736 MeV, 48.1 to 38.80 for 679 MeV, and 65.5 to 52.9° for 328 MeV) the polarization parameter show no clearly discernible increase that would be inconsistent with the shape of the polarization curve found by previous experiments in this energy range. We have retained the measurements of the polarization parameter for these angles although they are inherently less reliable.

Figure 18, which shows the plot of $P(\theta)$ at the energy of 328 MeV, contains also the values measured by Chamberlain et al.[12] in a double-scattering experiment. The agreement between the results of the two experiments might be regarded by some as evidence that our method of measuring the target polarization is satisfactory. Although we have not seen any reason to doubt this method, the agreement does represent our best check on our method of measuring target polarization.

In Fig. 22, the maximum value of the polarization parameter $P(\theta)_{max}$ has been plotted as a function of lab kinetic energy T_p. Values measured in other experiments are shown for comparison. The points plotted with an open circle in the energy region from 1.7 to 6.0 GeV are preliminary results as reported at the 1964 International Conference on High Energy Physics in Dubna.[13]

Since the purpose of this dissertation is to contribute data toward a future experimental determination of the two-nucleon isotopic spin-1 amplitude, it is worthwhile at this point to review the amount of data

needed for such a determination. From Eq. (II-12) one can see that, in principle, ten experiments at all angles are necessary to determine fully the ten parameters in the M matrix at one energy. However, in the energy region where the interaction is purely elastic, the fact that the scattering matrix is unitary gives conditions on the imaginary parts of the M matrix that reduce the number of independent parameters to 5. When inelastic processes become possible, the additional states resulting from inelastic scattering (about which it is difficult to get the needed experimental evidence) must be included or the unitarity condition would be incorrect.

The analysis of experimental data at many angles is usually accomplished by means of a phase-shift analysis. In terms of this description, the number of parameters needed to specify the scattering is a function of the maximum orbital angular momentum L_{max} that is considered important in the scattering.

In p-p scattering, the possible states of total spin can be described as a singlet and a triplet state. Since the two protons are identical fermions, the total wave function of the system must be antisymmetric, and this restricts the singlet state to occurring only in total states with even values of orbital angular momentum and the triplet state only with odd values of orbital angular momentum. Conservation of the total angular momentum J and conservation of spatial parity then require that the only allowable transitions occur between the following states:

$$\text{singlet } J=L \rightarrow \text{singlet } J=L$$
$$\text{triplet } J=L \rightarrow \text{triplet } J=L$$
$$\text{triplet } J=L+1 \rightarrow \text{triplet } J=L+1$$
$$\text{triplet } J=L-1 \rightarrow \text{triplet } J=L-1$$
$$\text{triplet } J=L+1 \leftrightarrow \text{triplet } J=L-1$$

where L is the orbital angular momentum (that the triplet transitions $J=L+1 \rightarrow J=L-1$ and $J=L-1 \rightarrow J=L+1$ are equal is a result of the assumption of time-reversal invariance). By counting, one can ascertain that

five parameters are needed for each two values of L. These are usually expressed as four phase shifts and a mixing parameter between states of the same total angular momentum, total spin, and spatial parity. When the inelastic processes occur, the parameters can become complex. Thus one needs $(5\ L_{max}/2)$ or $((5\ L_{max}+3)/2)$ parameters for L_{max} even or odd to obtain a phase-shift solution. Chamberlain et al.[12] have summarized the number of experimental parameters obtainable in some common forms of experiments with polarized protons. They conclude that in the elastic-energy region, five kinds of experiments, which include the differential cross section and polarization measurements, should determine the nuclear-phase shifts. In the inelastic-energy region, additional information on the effects of the inelastic processes is needed. In the phase-shift analyses performed by Zul'karneeve and Silin[13] and by Hoshizake and Machida[14] at 660 MeV, the assumption was made that the inelastic effects occur predominately in the lower angular-momentum states. The resonance model of Mandelstam for pion production at energies from 400 to 900 MeV was then used to estimate these contributions. At the time of the writing of this dissertation, not enough experiments have been done at the energies of 614, 679, and 736 MeV to be able to perform phase-shift analyses. The phase-shift analyses at 315 MeV are well known.[15]

In concluding this dissertation, we wish to express the thought that extensive experimental work will continue to be needed on the two-nucleon interaction to describe fully the spin-dependence of the forces. Any future theory, which might draw upon such an experimental description, will certainly need such work for quantitative comparison in order that the validity of the theory might be established. The polarized target is an important tool that will facilitate the execution of the needed spin-dependent experiments.

Table VIII. Polarization parameter $P(\theta)$ in elastic p-p scattering for incident lab kinetic energy of 328± 6 MeV.[a]

$-t[(\frac{BeV}{c})^2]$ ± 0.006	$\theta_{c.m.}$ ± 1°	$P(\theta)$	$\Delta P(\theta)$
0.107	49.1	0.389	0.045
0.119	52.2	0.349	0.031
0.133	55.3	0.324	0.025
0.147	58.4	0.317	0.022
0.162	61.6	0.255	0.020
0.177	64.8	0.256	0.027
0.193	68.1	0.191	0.024
0.210	71.4	0.165	0.023
0.227	74.7	0.187	0.023
0.283	85.3	0.163	0.035
0.302	88.9	0.016	0.027
0.322	92.6	-0.008	0.025
0.343	96.5	-0.054	0.024
0.365	100.6	-0.094	0.027

[a] A systematic error of $(^{+6.5}_{-5.8}\%)$ must be added in quadrature to the above errors $\Delta P(\theta)$.

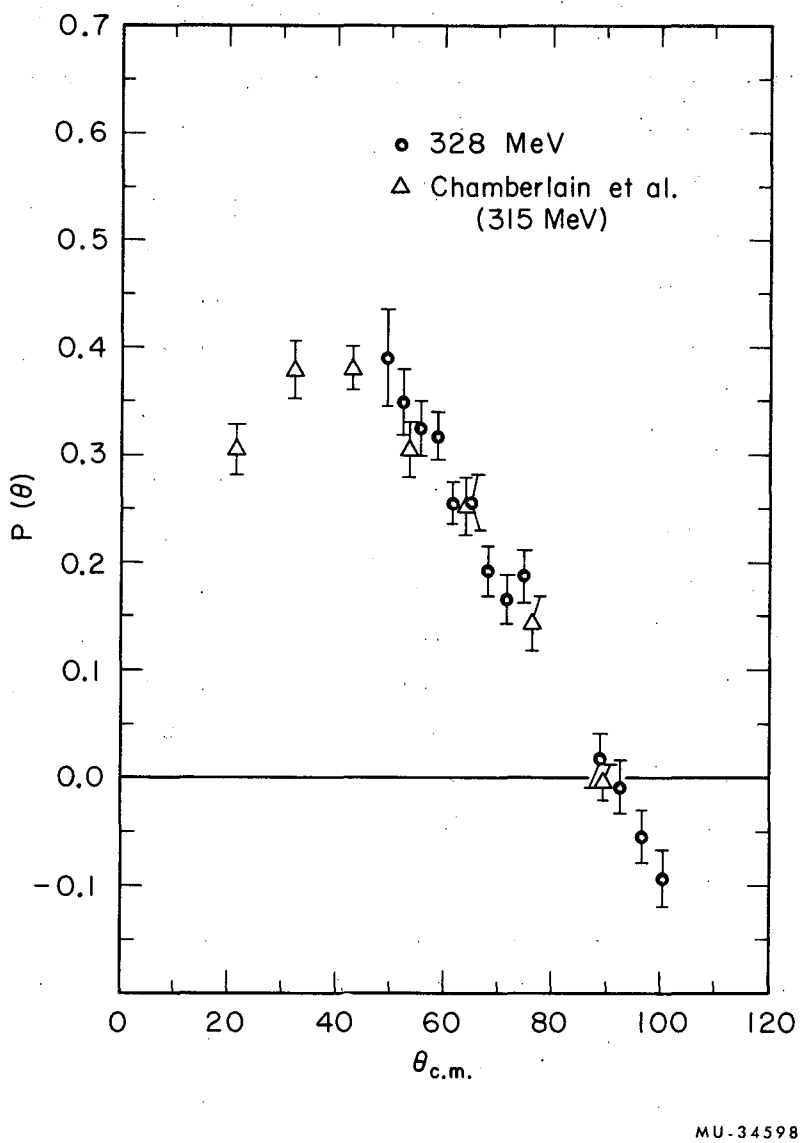

Fig. 18. The measured values of $P(\theta)$ in p-p scattering at 328 MeV are plotted as solid circles. The errors shown do not include systematic errors. The open triangles present data from Ref. 12.

Table IX. Polarization parameter $P(\theta)$ in elastic p-p scattering for incident lab kinetic energy of 614± 5 MeV.[a]

$-t[(\frac{BeV}{c})^2]$ ±0.015	$\theta_{c.m.}$ ±2°	$P(\theta)$	$\Delta P(\theta)$
0.271	58.0	0.505	0.019
0.313	62.8	0.492	0.019
0.344	66.2	0.413	0.020
0.356	67.5	0.463	0.019
0.397	71.9	0.325	0.018
0.401	72.3	0.357	0.019
0.453	77.6	0.238	0.016
0.511	83.5	0.091	0.015

[a] A systematic error of (± 19%) must be added in quadrature to the above errors $\Delta P(\theta)$.

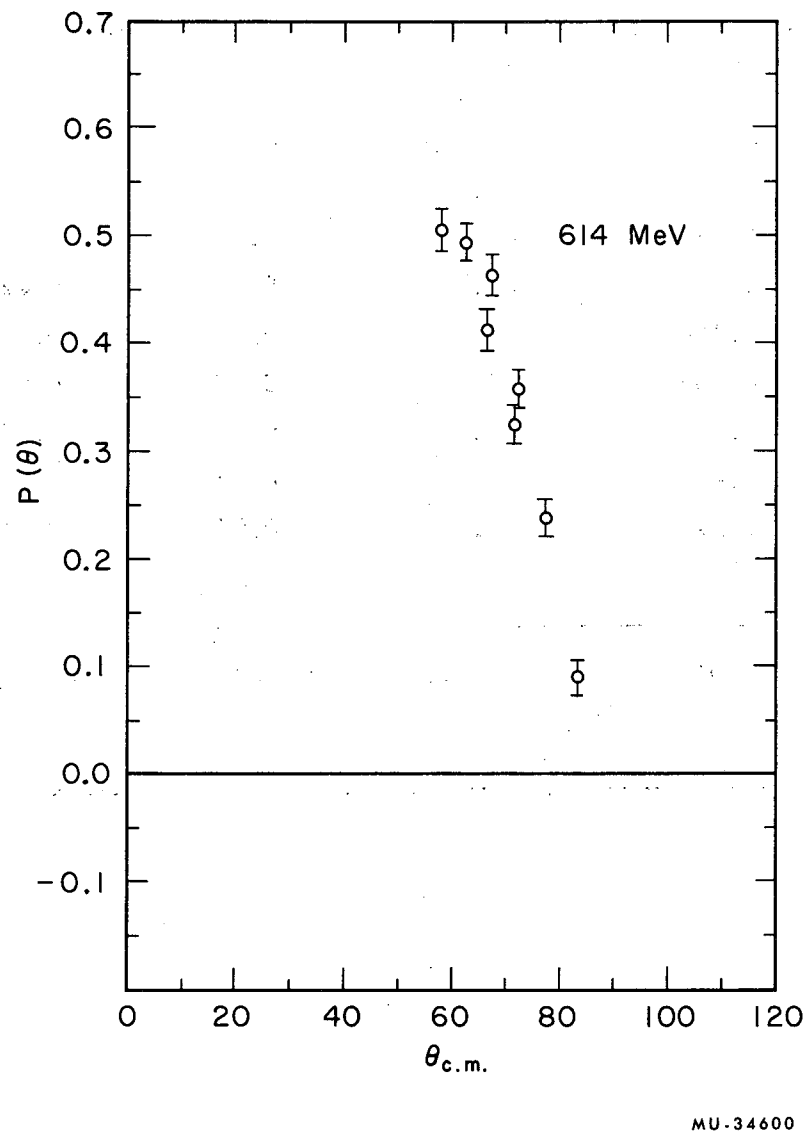

Fig. 19. The measured values of $P(\theta)$ in p-p scattering at 614 MeV. The errors shown do not include systematic errors.

Table X. Polarization parameter $P(\theta)$ in elastic p-p scattering for incident lab kinetic energy of 679 MeV.[a]

$-t[(\frac{BeV}{c})^2]$ ±0.01	$\theta_{c.m.}$ ±1°	$P(\theta)$	$\Delta P(\theta)$
0.141	38.8	0.578	0.028
0.163	41.9	0.578	0.019
0.186	45.0	0.583	0.017
0.212	48.1	0.596	0.017
0.238	51.2	0.570	0.013
0.266	54.3	0.529	0.013
0.294	57.4	0.484	0.018
0.324	60.5	0.430	0.017
0.354	63.7	0.399	0.018
0.386	66.7	0.363	0.019
0.427	70.8	0.293	0.030
0.458	73.7	0.274	0.027
0.490	76.7	0.247	0.031
0.522	79.6	0.151	0.036
0.555	82.6	0.073	0.044

[a] A systematic error of $(^{+6.5}_{-5.8}\%)$ must be added in quadrature to the above errors $\Delta P(\theta)$.

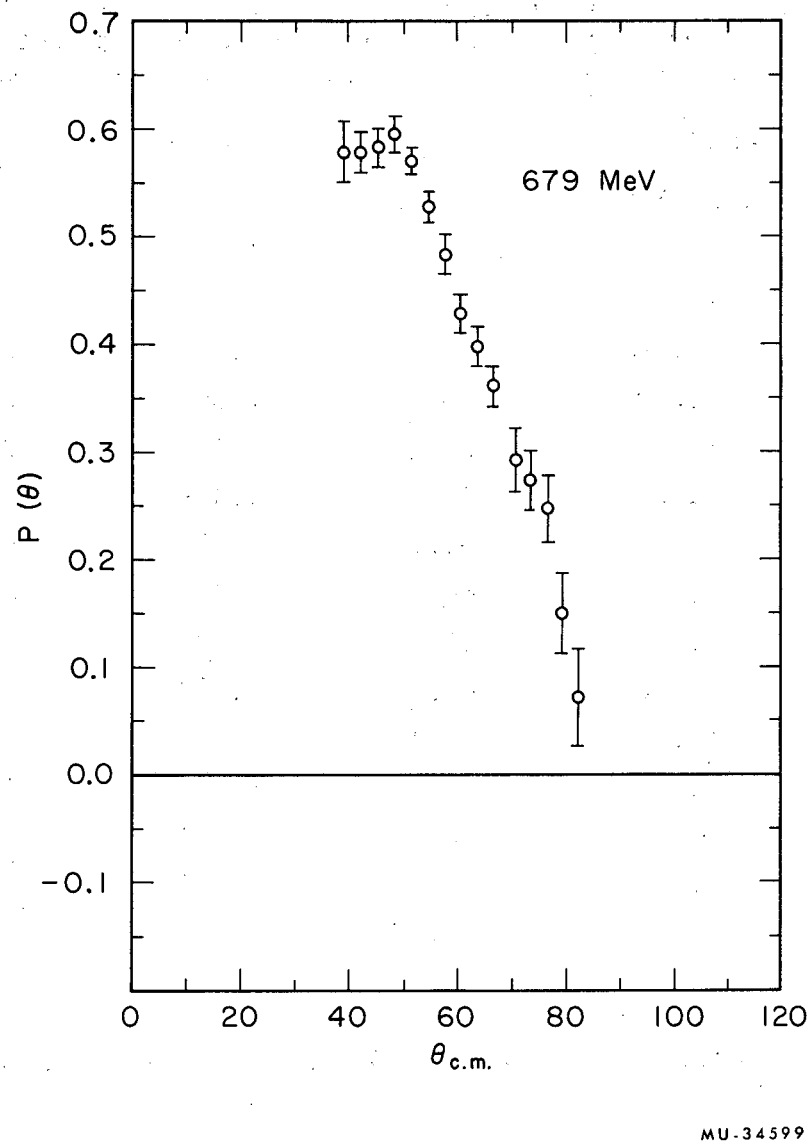

Fig. 20. The measured values of $P(\theta)$ in p-p scattering at 679 MeV. The errors shown do not include systematic errors.

Table XI. Polarization parameter $P(\theta)$ in elastic p-p scattering for incident lab kinetic energy of 736 MeV. [a]

$-t[(\frac{BeV}{c})^2]$ ±0.01	$\theta_{c.m.}$ ±1°	$P(\theta)$	$\Delta P(\theta)$
0.108	32.5	0.579	0.049
0.129	35.6	0.579	0.028
0.152	38.8	0.553	0.017
0.177	42.0	0.560	0.014
0.203	45.1	0.559	0.015
0.231	48.3	0.528	0.011
0.260	51.4	0.520	0.011
0.291	54.6	0.497	0.013
0.322	57.7	0.498	0.013
0.354	60.9	0.473	0.014
0.404	65.5	0.419	0.018
0.437	68.4	0.365	0.017
0.470	71.4	0.342	0.018
0.504	74.3	0.304	0.018
0.538	77.2	0.231	0.018
0.573	80.2	0.180	0.018
0.609	83.2	0.144	0.023

[a] A systematic error of $(^{+6.5}_{-5.8})$ % must be added in quadrature to the above errors $\Delta P(\theta)$.

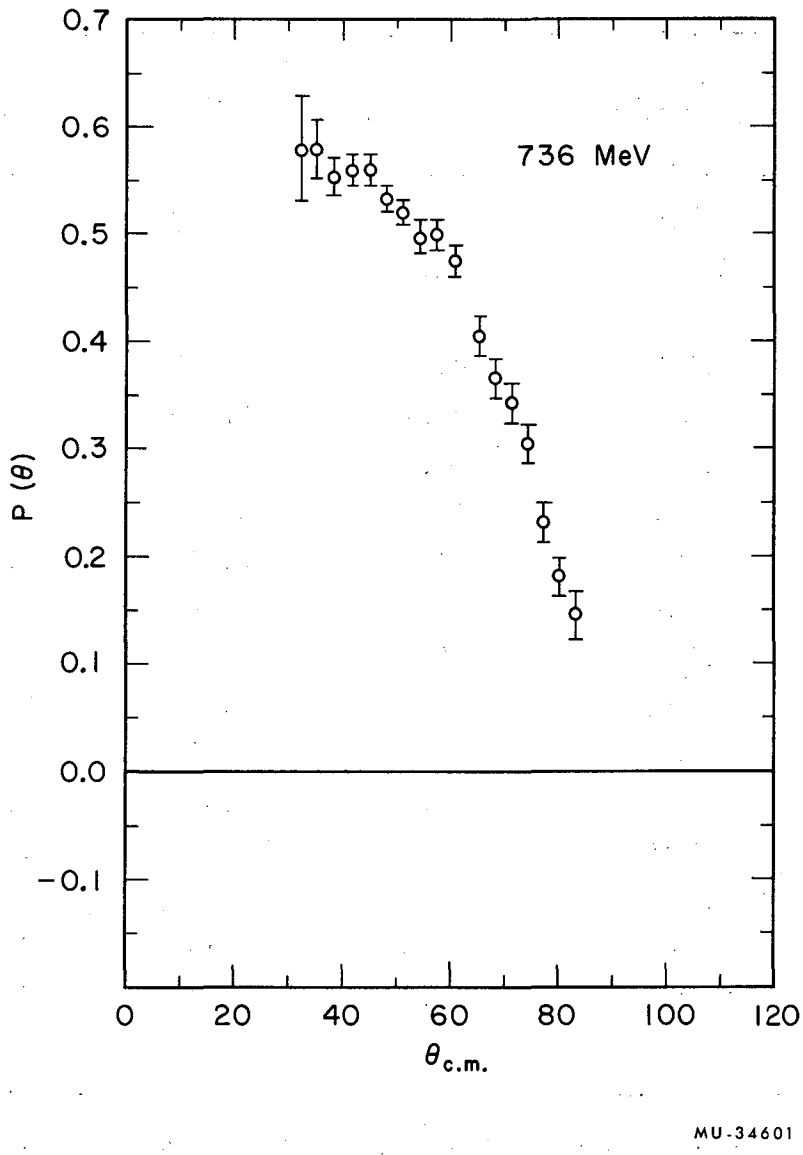

Fig. 21. The measured values of P(θ) in p-p scattering at 736 MeV. The errors shown do not include systematic errors.

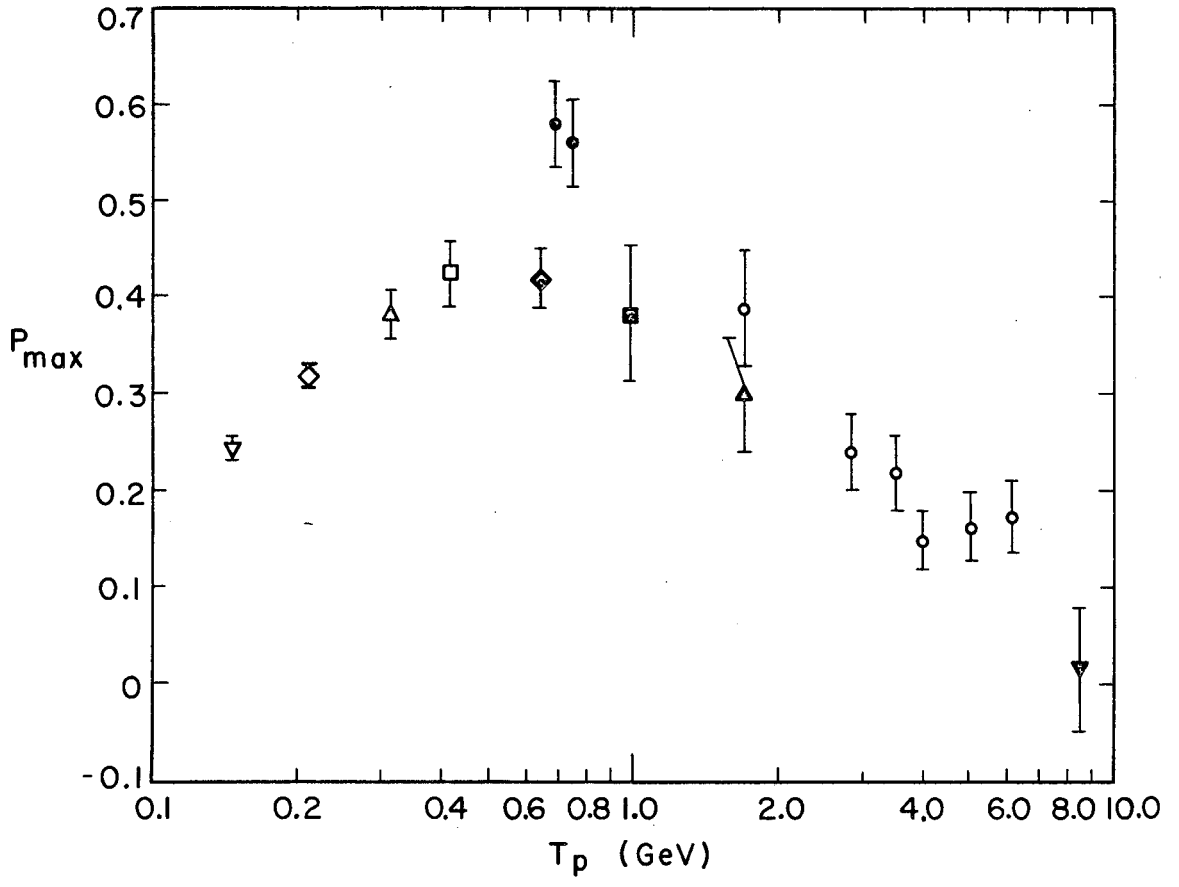

MUB-3318

Fig. 22. Maximum polarization as a function of beam energy T_p. Values from this experiment include systematic error. ⊙, data from this experiment; O, data from Ref. 16; ▽, data from Ref. 17; ◇, data from Rev. 18; △, data from Ref. 12; □, data from Ref. 19; ◈, data from Ref. 20; ▣, data from Ref. 21; ▲, data from Ref. 22; ▼, data from Ref. 23.

ACKNOWLEDGMENTS

I wish to express my deep gratitude to Professor Owen Chamberlain, who supervised my graduate research. His instruction, suggestions and ideas, criticism, and integrity have been to me an invaluable guide.

I wish to thank Professor Gilbert Shapiro for his very great contributions to the experiment in terms of design, analysis, personal effort, and encouragement.

I thank very much my fellow graduate student and good friend, Helmut Dost. In addition to many other contributions, the design of the beam, much of the mechanical structure, and the conversion of the data to a processable form were primarily due to his efforts.

To Dr. Claude Schultz and Dr. Leland Holloway I wish to express my gratitude for their help during the experiment. In addition, I wish to express my gratitude to my fellow students, John Arens, Paul Grannis, Michel Hansroul, and Claiborne Johnson, for their many efforts and contributions to this experiment.

I thank Wladyslaw Troka for his help and, even more, for his good companionship and enlightening discussions during our mutual period of graduate research.

I wish to thank Professor Herbert Steiner for his instruction and advice.

The successful completion of this experiment was also due to many other people at this Laboratory: the cyclotron crew under Mr. James Vale and Mr. Lloyd Hauser; the accelerator technicians under Mr. Louis Sylvia and Mr. Robert Walton, and the physics technical support people under Mr. Lee Wagner.

As all human endeavors, research also takes place not in isolation. Indirect contributions are immense and immeasurable. I wish to thank my wife, Nancy.

This work was done under the auspices of the U. S. Atomic Energy Commission.

REFERENCES

1. M. H. MacGregor, M. J. Moravcsik, H. P. Stapp, Ann. Rev. Nucl. Sci. 10, 291 (1960).
2. W. H. Hess, Rev. Mod. Phys. 30, 368 (1958).
3. L. Wolfenstein, Ann. Rev. Nucl. Sci. 6, 43 (1956).
4. L. Wolfenstein, J. Ashkin, Phys. Rev. 85, 947 (1952).
5. R. H. Dalitz, Proc. Phys. Soc. (London) A65, 175 (1952).
6. H. P. Stapp, Phys. Rev. 103, 425 (1956).
7. M. Rich and R. Madey, Range-Energy Tables, UCRL-2301, 1954 (unpublished).
8. C. H. Schultz, Scattering of 250-MeV Positive Pi Mesons from a Polarized Target (Ph. D. Thesis), UCRL-11149, January 1964 (unpublished).
9. C. D. Jeffries, Dynamic Nuclear Orientation (Interscience Publishers, Inc., New York, 1963); A Abragam, The Principles of Nuclear Magnetism (Clarendon Press, Oxford, 1961); and other references quoted therein.
10. C. D. Jeffries, op. cit., p. 14.
11. G. Shapiro, Polarized Targets, in Nuclear Techniques and Instrumentation, Vol. 1 (North-Holland Publishing Co., Amsterdam, 1964).
12. O. Chamberlain, E. Segrè, R. D. Tripp, C. Wiegand, and T. Ypsilantis, Phys. Rev. 105, 288 (1957).
13. R. Ya. Zul'karneev and I. N. Silin, Phys. Letters 3, 265 (1963).
14. N. Hoshizaki and S. Machida, p-p Scattering at 660 MeV, preprint, Research Institute of Fundamental Physics, Kyoto University, Kyoto, Japan (unpublished).
15. H. P. Stapp, T. J. Ypsilantis, and N. Metropolis, Phys. Rev. 105, 302 (1957); M. H. MacGregor, M. J. Moravcsik, and H. P. Stapp, Phys. Rev. 116, 1248 (1959).

16. H. M. Steiner, F. W. Betz, O. Chamberlain, B. D. Dieterle, P. D. Grannis, C. H. Schultz, G. Shapiro, L. Van Rossum, D. M. Weldon, Polarization in Proton-Proton Scattering Using a Polarized Target, Part II, in Proceedings of the 1964 International Conference on High Energy Physics, Dubna, U. S. S. R., August 5-15, 1964 (to be published).
17. J. N. Palmieri, A. M. Cormack, N. F. Ramsey, and R. Wilson, Ann. Phys. (N. Y.) 5, 299 (1958).
18. J. Tinlot and R. E. Warner, Phys. Rev. 124, 890 (1961).
19. J. A. Kane, R. A. Stallwood, R. B. Sutton, T. M. Fields, J. G. Fox, Phys. Rev. 95, 1694 (1954).
20. M. G. Mescheryakov, S. B. Nurashev, G. D. Stoletov, Zh. Eksperim. i. Teor. Fiz. 33, 37 (1957).
21. R. J. Homer, W. K. MacFarlane, A. W. O'Dell, E. J. Sacharidas, and G. H. Eaton, Nuovo Cimento 23, 690 (1962).
22. P. Bareyre, J. F. Detoef, L. W. Smith, R. D. Tripp, and L. Van Rossum, Nuovo Cimento 20, 1049 (1961).
23. V. P. Kanavets, I. I. Levintov, B. V. Morozov, M. D. Shafranov, Zh. Eksperim. i. Teor. Fiz. 45, 1272 (1963).